Measurement Technique and Thermodynamic Modeling on Trace Mercury in Natural Gas and Its Production Facilities

June 2022

Junya YAMADA

Measurement Technique and Thermodynamic Modeling on Trace Mercury in Natural Gas and Its Production Facilities

A Dissertation Submitted to
the School of the Integrative and Global Majors,
the University of Tsukuba
in Partial Fulfillment of the Requirements
for the Degree of Doctor of Philosophy in Environmental Management
(Doctoral Program in Life Science Innovation)

Junya YAMADA

Abstract

Two types of apparatus were developed using cold vapor atomic absorption spectroscopy with a wavelength of 253.7 nm to investigate mercury (Hg) concentration at the ppm to ppb levels. This investigation was explicitly interested in natural gas components and gas processing chemicals used in acid gas removal units and dehydration units in gas processing facilities.

The Hg solubility in gaseous methane, ethane, carbon dioxide, and artificial natural gas was investigated by a flow-type apparatus at 268.15 to 303.15 K and up to 6.042 MPa. The mole fraction of Hg ranged from 4.842×10^{-9} to 8.103×10^{-7} in the vapor phase and decreased with the pressure. Under the isobaric condition, the mole fraction of Hg increased with the temperature and followed the van't Hoff equation. The dissolution enthalpies were almost the same among these gases. Moreover, the enthalpies were the same as the enthalpy of vaporization of Hg. These results suggested that Hg and gas molecules will be isolated and the interaction between Hg and gas molecules will be weak.

The Hg solubility in methanol, mono-ethylene glycol, diethylene glycol, triethylene glycol, and *N*-methyldiethanolamine was measured at 298.2 to 333.4 K under atmospheric pressure of nitrogen. The mole fraction of Hg in these solvents ranged from 5.65×10^{-8} to 6.34×10^{-7} and increased with the temperature Moreover, it also followed the van't Hoff equation. The dissolution enthalpies were far smaller than that in the isobaric gases. At the isothermal condition, the mole fraction of Hg was proportional to the number of their constituent atoms. This relationship could be applied to C5 to C8 and C10 of aliphatic hydrocarbons. It can predict the Hg solubility in heavy hydrocarbons in natural gas and oil.

The Peng-Robinson equation of state (PR-EOS) could be applied to correlate the experimental data by optimizing of the attractive parameter through the saturated vapor pressure of Hg and with the assumption that the liquid Hg phase was a solid with fluidity. The experimental data were well correlated and predicted with the PR-EOS just by the binary interaction parameters with temperature dependence.

Table of Contents

List of Abbreviations

ARLD	average relative logarithmic deviation
CPA-EOS	cubic plus association equation of state
CVAAS	cold vapor atomic absorption spectroscopy
DEG	diethylene glycol
DIPPER	design institute for physical properties
EOS	equation of state
LLE	liquid- liquid equilibrium
LNG	liquified natural gas
MDEA	*N*-methyldiethanolamine
MEG	mono-ethylene glycol
PR-EOS	Peng-Robinson equation of state
PRSV-EOS	modified version of Peng-Robinson equation of state by Stryjek and Vera
SVE	solid-vapor equilibrium
TEG	triethylene glycol
VLE	vapor-liquid equilibrium
VLLE	vapor-liquid-liquid equilibrium

List of Figures and Tables

Chapter 1 Introduction

1.1 Background of research

Mercury (Hg) is a six-period metal, with the atomic number 80. Hg has similar characteristic as novel metals like gold and platinum; it can be recovered from mines in its pure elemental form. Elemental Hg also has interesting physical properties. For example, it is liquid under standard atmospheric pressure and room temperature, a property not found in other metals. Since the third century before Christ, liquid elemental Hg had been employed as a raw material for pigments in ancient China. Therefore, Hg is easy to convert to oxide, sulfide and chlorides, and giving vivid red, black, and white colors, respectively. In addition, its bactericidal property was believed to provide an eternal life to ancient Chinese Emperors. After developing electricity in the 20th century, the high electric conductivity received attention for its application in electric devices such as lumps, switches, relays, and sensors. Many researchers reported many specific physical and chemical properties of Hg, and these data are utilized in industry for thermometers, sanitizers, medical drugs, and catalysts. However, the usage of Hg was decreased, because of neurological disorders peculiar to Hg poisoning; this severe disease caused by the bioaccumulation of Hg in 1960s Japan was called "Minamata disease." The industrial wastewater containing methylmercury compounds were discharged into the Minamata Bay, and the methylmercury compounds were bioaccumulated in shellfishes and fishes. Consequently, serious neurological disease occurred in the people who ate these seafoods. Since the industry put corporate profits before investigating cause of the mercury pollution, a number of victims continued to increase, and the injury extended to the victim's children. The relief for the victims continues even over 60 years later of the Minamata disease occurred. After the severe environmental pollution, the research topics were rapidly shifted from physical to analytical chemistry. Now ppm to ppb levels of Hg can be precisely detected by high sensitivity analyzers, and these analytical methods have been applied to environmental science and research.

In the oil and gas industry, it is well known that trace amounts of Hg are found in raw and untreated oil and gas produced from in-situ reservoirs. Mercury in natural gas can cause amalgam

corrosion or liquid metal embrittlement of aluminum heat exchangers in liquefied natural gas (LNG) plants. Consequently, natural gas processing facilities suffer severe damage to process equipment, causing unwanted shutdowns. The first reported incident caused by Hg in natural gas occurred in Skikda LNG, Algeria, in 1987 [1]. The other incident related to Hg in natural gas and oil occurred elsewhere from the 1980s to the 2000s [2, 3, 4, 5]. Hg in condensate and crude oil can also cause the poisoning of precious metal catalysts used in oil refineries and petrochemical manufacturers. For this reason, it is difficult for oil producers to sell crude oil and condensate with high mercury content to those customers; consequently, oil producers are forced to discount the sales price of crude oil and condensate [6].

Furthermore, there is a risk of mercury emissions from oil and gas production facilities to the environment. **Fig. 1.1** shows the global cycle of Hg assessed by the United Nations Environment Programme (UNEP) [7]. Emission sources of Hg to the atmosphere include geogenic, burning biomass, soil and vegetation, and anthropogenic. The UNEP identified primary anthropogenic five major emission sources: coal combustion, cement burning, non-ferrous metal refinery, waste burning, and artisanal small-scale gold mining. Governments that have a treaty with the UNEP Minamata Convention are working to reduce Hg emission from those five emission sources. The Hg emissions from the oil and gas industry are divided into upstream (oil and gas production) and downstream (oil refinery) emissions. The Hg emission from upstream is not quantified by the UNEP [8], while that from downstream is assumed to be less than 1 % of the total global anthropogenic emission to air [8]. Although the oil and gas industry is not a primary source of Hg, managing Hg emissions from this industry is crucial to prevent environmental pollution. Proper handling and removal of Hg during gas and oil production are important responsibilities of the oil and gas industries to prevent health, safety, and environmental issues. Hg in natural gas and oil is usually removed by commercial mercury adsorbents packed in the mercury removal unit (MRU). It is vital to know the Hg distribution in natural gas processing facilities for proper MRU management and design optimization. However, there are some technical challenges because field measurement of Hg sometimes indicates abnormal

values due to contamination and adsorption of Hg in sampling valves in the facility or sample chambers. A numerical prediction model that can accurately predict Hg distribution in production facilities is needed to address the problem.

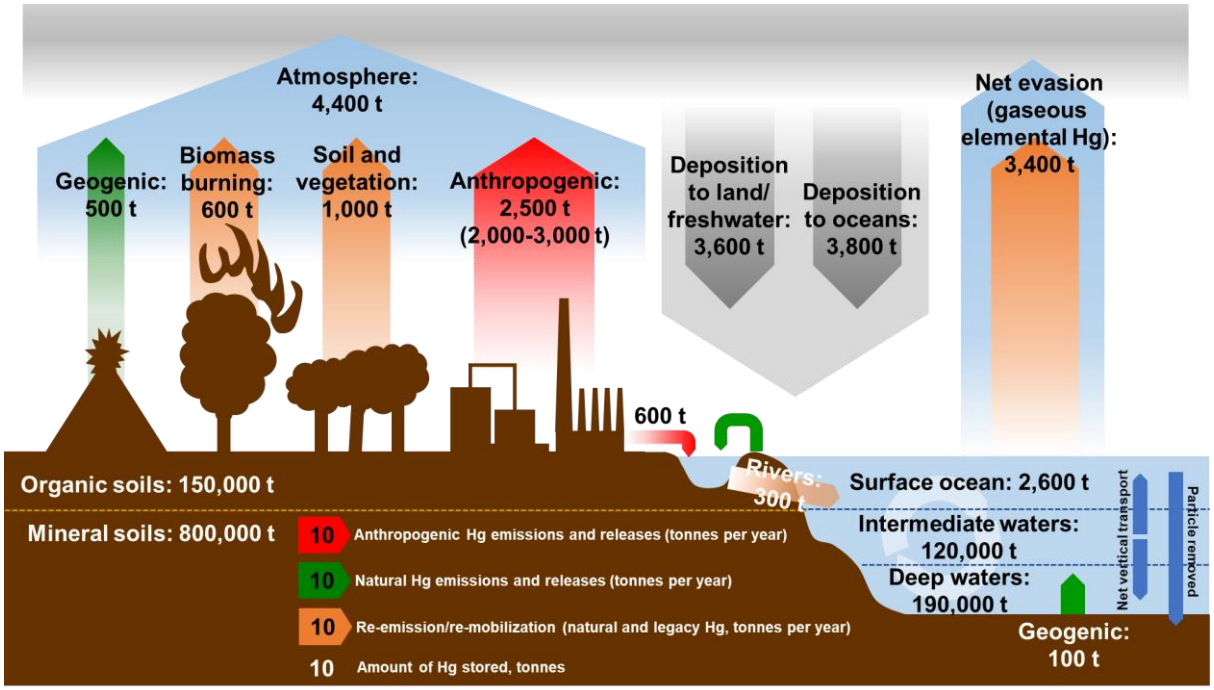

Fig. 1.1. Global mercury cycle (made from UNEP Global Mercury Assessment 2018 [7])

1.2 Objectives of doctoral research

In this doctoral research, three primary objectives are set as follows:

1) Experimentally investigate Hg solubility in gaseous natural gas components, including methane, ethane, and carbon dioxide. Minimal literature values exist within the typical operating pressure and temperature ranges of natural gas processing facilities.
2) Experimentally investigate Hg solubility in solvents for natural gas processing, which are mono-ethylene glycol (MEG), diethylene glycol (DEG), triethylene glycol (TEG), and *N*-methyldiethanolamine (MDEA). Again, very few literature values exist within the necessary ranges.
3) Establish a prediction model capable of calculating Hg distribution in natural gas processing facilities using literature and experimental data for Hg solubility in vapor and

liquid phases, which can be easily implemented on commercial process simulators.

1.3 Composition of doctoral thesis

This doctoral thesis consists of six chapters.

Chapter 1 is the introduction of the doctoral thesis. The background and the issues related to Hg in oil and gas are outlined. Then, the objectives and the composition of the doctoral research were explained in this Chapter.

Chapter 2 contains a literature review, helping to identify the doctoral research objectives. Previous studies about Hg solubility measurements for vapor and liquid phases are reviewed. Then, insufficient datasets previously used to predict Hg distribution in natural gas processing facilities were identified. In addition, the chosen prediction model for the Hg soolubility in vapor and liquid phases is discussed in the context of previous research.

Chapter 3 is the experimental section. The experimental apparatus for Hg solubility measurements for vapor and liquid phases are described. Then, the method for the data correlation and prediction of Hg solubility is introduced.

Chapter 4 investigates the Hg solubility in gaseous natural gas components: methane, ethane, and carbon dioxide. The results of the Hg solubility measurement, and the data correlation, and the prediction by a modified cubic equation of state (EOS) model are also discussed.

Chapter 5 investigates the Hg solubility in solvents for natural gas processing: methanol, MEG, DEG, TEG, and MDEA. The Hg solubility in methanol was measured as the validation of the experimental apparatus. MDEA is widely used for acid gas removal and MEG, DEG and TEG are used for dehydration in natural gas processing. The results of the Hg solubility measurement are explained, and the data correlation and the prediction by the modified cubic equation of state model are also discussed. In addition, the relationship between the Hg solubility and the number of constituent atoms of solvents explored.

Chapter 6 is the conclusion. The results and findings of this research are summarized, then

future research directions and further challenges are explained.

This research will contribute to reduce Hg pollution to air and water during natural gas processing and help prevent Hg disasters such as the Minamata disease.

Chapter 2 Reviews of Measurements and Modeling of Hg in Vapor and Liquid Phases

This chapter provides an overview of previous research on measurement and modeling of Hg partitioning in vapor and liquid phases. The main purpose of the literature review is to survey previous studies and to find problems and insufficiency of their research.

2.1 Methods of Hg solubility measurements

Richardson and Rowlinson [9] conducted the Hg solubility measurement in the vapor phase by a static method where they introduced the elemental Hg into a small reservoir and weighed it before and after the equilibrium. The weight loss of Hg was evaluated as the amount of Hg to vapor phase. Jepson et al. [10] also employed a static method where the drop of ^{203}Hg was enclosed in a glass tube. They measured the gamma-ray of ^{203}Hg in the vapor phase from the tube. Butala et al. [11] developed the apparatus based on the flow method. The apparatus had the pre-saturation cell and the Hg saturation cell to achieve the supersaturated condition in the saturation cell. Chapoy et al. [12] also used a similar flow type apparatus to Butala et al. However, contact methods between Hg and gases in the saturation cell were not mentioned in their work.

Regarding methods for Hg solubility measurement in the liquid phase, a static method was widely employed by Klehr and Voigt [13], Kuntz and Mains [14], Choi and Tuck [15], Spencer and Voigt [16], Glew and Hames [17], Vogel and Gjaldebaek [18], Onat [19], Sorokin et al. [20], Okouchi and Sasaki [21, 22], Migdisov et al. [23], Miedaner et al. [24], Bloom and Gallup [25], Gallup et al. [26], and Marsh et al. [27]. However, Corns et al. [28] conducted Hg solubility measurements using a flow method where the saturated Hg vapor continuously flowed into solvents until reaching equilibrium. Some researchers added a small amount of reducing agents to solvents to prevent the oxidation of elemental Hg. Sanemasa [29] and Li et al. [30] employed a closed-loop apparatus.

Regarding Hg detection methods, spectroscopic methods were widely employed by many researchers, including cold vapor atomic absorption spectroscopy (CVAAS) with the wavelength of

253.7 nm [11, 12, 14, 17 to 22, 29, 30] and cold vapor atomic fluorescence spectroscopy (CVAFS) [25, 26, 28]. Additionally, Marsh et al. [27] developed a laser-based technique utilizing two-photon excitations at 320.782 nm and 546 nm to measure Hg solubilities below 298 K. Radiation measurement was employed by some researchers, using radioactive Hg, ^{203}Hg, as the source. Jepson et al. [10] employed a Geiger counter to detect the gamma-ray from ^{203}Hg, which was used as a tracer. Klehr and Voigt [13] and Spencer and Voigt [16] used a single-channel scintillation counter in which the window width was adjusted to count only the photopeak at 279 keV. Migdisov et al. [23] and Miedaner et al. [24] performed Hg solubility measurements by a gravimetric method. They measured mass loss of elemental Hg in the equilibrium cell before and after the experiments by an analytical balance to evaluate Hg solubilities in solvents.

2.2 Saturated vapor pressure of Hg

There is much data on the saturated vapor pressure of Hg by researchers. Huber et al. [31, 32] summarized the previous data and proposed an empirical equation as the modified version of the Wagner equation. It can be argued that the Wagner equation is the empirical principle of corresponding states. Although the Huber equation can accurately correlate saturated vapor pressure of Hg, six fitting parameters are needed. Before the equation by Huber et al., a simplified Antoine equation was proposed by Dumarey in the 1980s. This equation is commonly known as the Dumarey equation [33] and is recommended for use as the calibration standard in the standard method of determining Hg concentration in natural gas, ISO 6978-2:2003 [34]. However, the Dumarey equation differs from the Huber equation by more than 7% at 20 °C [35].

Recently, another approach using cubic EOS was proposed. Edmonds et al. [36] first proposed a cubic EOS to predict saturated pressure and Hg solubility in aliphatic hydrocarbons. They demonstrated that the advanced Soave-Redlich-Kwong EOS could reproduce the value of the Huber equation by adding temperature dependence to the parameter in their EOS model. However, the details of modification to the EOS were not disclosed. Smit et al. [37] proposed the Shell's Modified

and Improved Redlich-Kwong EOS, which includes specified pure component parameters to calculate a good description of the vapor pressure of Hg. Unfortunately, they also did not explain the details of their modification. Mentzelos [38] presented the Peng-Robinson equation of state (PR-EOS), which can reproduce the value of the vapor pressure of Hg in the Design Institute for Physical Properties (DIPPER) when the Matias-Copemen alpha function was implemented to the PR-EOS and correlated with the DIPPER in his Diploma Thesis. This result was published by Koulocheris et al. [38]. Although the PR-EOS with the Matias-Copeman can accurately calculate the saturated vapor pressure of Hg, three pure component parameters must be correlated with the experimental data. A more simplified prediction model for the saturated vapor pressure of Hg is preferred in practical use.

2.3 Measurement of Hg solubility in vapor phase

Although several researchers investigated Hg solubility in the vapor phase, few datasets are available. Focusing on the natural gas components, Hg solubility in methane, ethane, propane, carbon dioxide, and nitrogen has been reported.

2.3.1 Methane

Figure 2.1 shows the reported Hg solubility in methane by Butala et al. [11] and Chapoy et al. [12]. Butala et al. [11] firstly reported the Hg solubility in methane at nine isotherms between 253.15 K and 293.15 K, and the pressure conditions were 400 psia (2.76 MPa), 500 psia (3.45 MPa), and 1000 psia (6.89 MPa). They employed a flow-type apparatus and measured the Hg solubility in methane, ethane, propane, carbon dioxide, a binary gas mixture of propane (59.4 mole%) and iso-butane (40.6 mole%), and a three components mixture of n-butane (32.4 mole%) + n-pentane (33.5 mole%) + n-hexane (34.1 mole%). Although they conducted comprehensive Hg solubility measurement for natural gas components, the temperature conditions, particularly in the high-temperature region, still did not extend to the operating condition of natural gas processing facilities. Most recently, Chapoy et al. [12] reported the Hg solubility in methane at temperatures between

244.35 K and 323.15 K and at pressure from 0.80 MPa to 18.62 MPa. They used a flow-type apparatus similar to Butala et al.

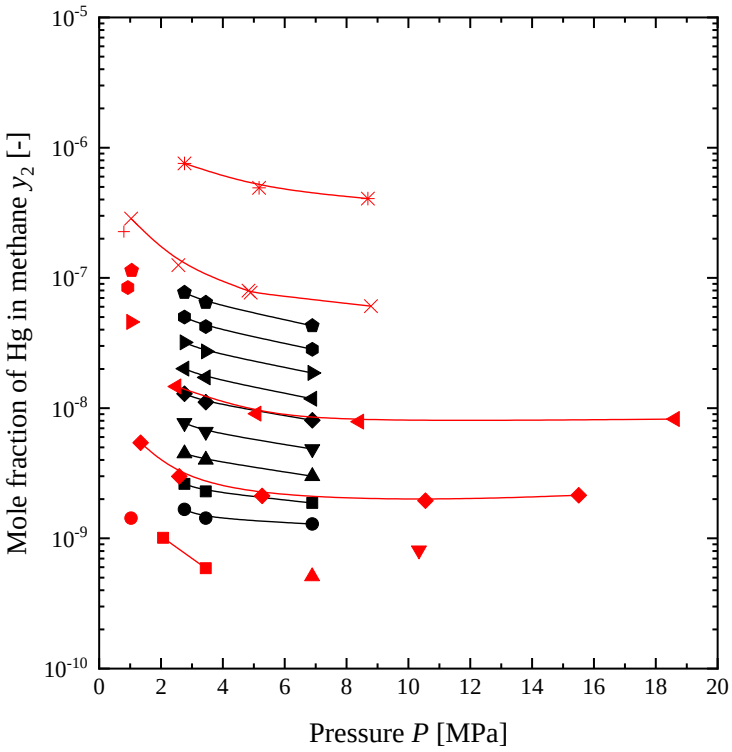

Fig. 2.1 Reported Hg solubility in methane: Butala et al. [11] at 253.15 K (●), 258.15 K (■), 263.15 K (▲), 268.15 K (▼), 273.15 K (◆), 278.15 K (◀), 288.15 K (▶), 293.15 K (⬟); Chapoy et al. [12] at 244.35 K (●), 244.55 K (■), 245.15 K (▲), 246.15 K (▼), 258.15 K (◆), 273.15 K (◀), 278.15 K (▶), 283.15 K (⬢), 288.15 K (⬟), 293.15 K (+), 298.15 K (×), 323.15 K (*).

2.3.2 Ethane

Koulocheris et al. [39] showed the vapor-liquid equilibrium (VLE) of an Hg-ethane system at five isotherms between 273 K and 293 K and pressure up to 37.7 bar (3.77 MPa); however, the exact values were not mentioned in the paper. The most recent data set was reported by Chapoy et al. [12] in both the VLE and the liquid-liquid equilibrium (LLE) condition. The temperature ranged between 244.1 K and 323.15 K, and the pressure ranged from 0.7 MPa to 11.38 MPa. **Figure 2.2** shows the Hg solubility in ethane reported by Chapoy et al. [12].

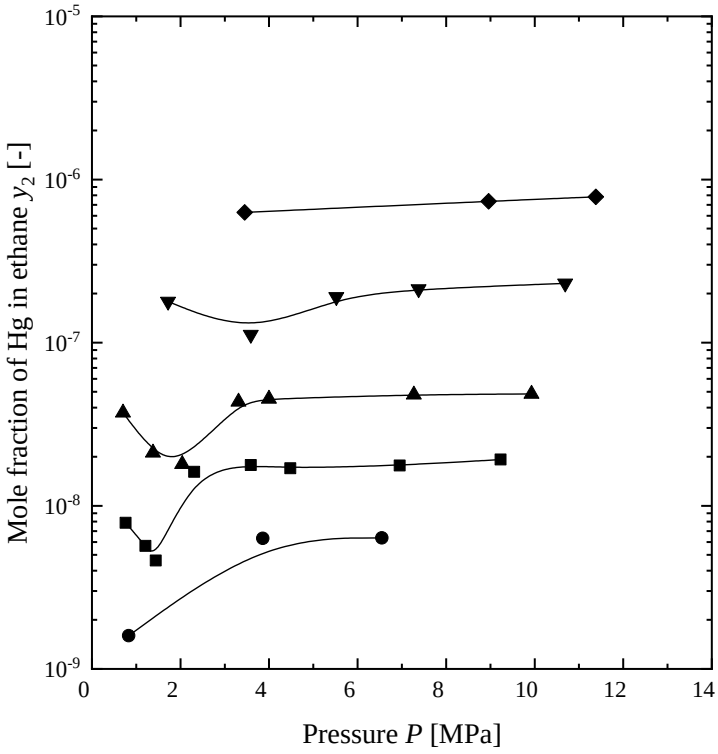

Fig. 2.2 Reported Hg solubility in ethane: Chapoy et al. [12] at 244.10 K (●), 258.15 K (■), 273.15 K (▲), 298.15 K (▼), 323.15 K (◆).

2.3.3 Propane

Jepson et al. [10] reported the VLE measurement on an Hg-propane system at three isotherms of 457.15 K, 491.15 K, and 529.15 K, and the pressure range was 0.001 MPa to 3.293 MPa. Similarly, Butala et al. [11] measured the mole fraction of Hg in the vapor and liquid phase at five isotherms between 273.15 K and 293.15 K at around 7.0 psia (0.048 MPa) below the saturation pressure of propane due to the pressure drop across the experimental apparatus. Therefore, they suggested that the Hg solubility in propane extrapolated to saturation pressure for each temperature. The most recent data was reported by Chapoy et al. [12]. They measured the mole fraction of Hg in the vapor and liquid phase of ethane at 246.65 K to 307.69 K and a pressure of 1.03 MPa to 3.45 MPa.

2.3.4 Butanes

Jepson et al. [10] measured the Hg solubility in n-butane at three isotherms, 457.15 K,

491.15 K, and 529.15 K, with pressures up to 3.1 MPa. Richardson and Rowlinson [9] also reported eleven isotherms between 486.05 K and 572.95 K and pressures up 38.5 MPa. For the Hg solubility in iso-butane, Butala et al. [11] only investigated the VLE and the LLE conditions at five isotherms from 263.15 K to 283.15 K and pressures up to 8.3 MPa.

2.3.5 Carbon dioxide

Butala et al. [11] first reported Hg solubility in carbon dioxide at five isotherms between 273.15 K and 293.15 K. As they measured Hg solubility at about 7 psia below the saturation pressure of carbon dioxide for the same reason as the case of propane, they suggested the extrapolated data of Hg solubility in carbon dioxide as the same manner of propane. The most recent data was measured by Chapoy et al. [12] at five isotherms between 234.15 K and 323.15 K. The pressure condition was from 0.39 to 13.79 MPa. **Figure 2.3** shows the reported Hg solubility in carbon dioxide.

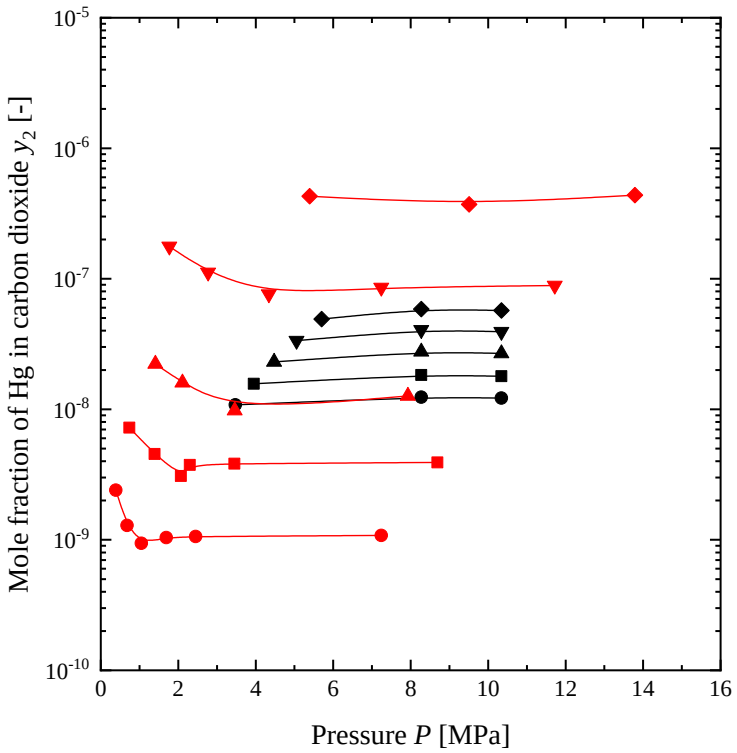

Fig. 2.3 Reported Hg solubility in carbon dioxide: Butala et al. [11] at 273.15 K (●), 278.15 K (■), 283.15 K (▲), 288.15 K (▼), 293.15 K (◆); Chapoy et al. [12] at 243.15 K (●), 258.15 K (■), 273.15 K (▲), 298.15 K (▼), 323.15 K (◆).

2.3.6 Nitrogen

Mentzelos [36] showed the six data points for the mole fraction of Hg in the vapor phase at 273.15 K, with pressure ranging from 7 to 67 bar (0.7 to 6.7 MPa). However, the exact values were not mentioned in the Diploma Thesis. Chapoy et al. [12] measured the most recent data at five isotherms between 244.35 K and 323.18 K, with pressure ranging from 0.70 to 17.28 MPa.

2.4 Measurement of Hg solubility in liquid phase

Compared with the dataset for the Hg solubility in the vapor phase, many datasets are available for the Hg solubility in the liquid phase. However, datasets about some solvents used in natural gas processing are extremely few or not available. The Hg solubility in the liquid phase related to natural gas processing is reviewed hereafter.

2.4.1 Aliphatic hydrocarbons

The Hg solubility in aliphatic hydrocarbons is available in a wide temperature range. Regarding the Hg solubility in pentanes, Marsh et al. [26] give data between 233 K and 383 K, while Okouchi and Sasaki [21] provide 278.15 K to 313.15 K, and Butala et al. [11] studied between 258.15 K and 293.15 K. Bloom and Gallup [25] and Kuntz and Mains [14] reported the Hg solubility in n-Pentane at 298.15 K. The Hg solubility in iso-Pentane was only reported by Kuntz and Mains [14] at 298.15 K.

Regarding the Hg solubility in hexanes, almost all data was reported by Okouchi and Sasaki [21] and Spencer and Voigt [16]. Okouchi and Sasaki [21] reported the solubility of mercury in n-hexane at six isotherms between 278.15 K and 313.15 K. Spencer and Voigt [16] measured at five isotherms between 273.15 K and 308.15 K. Other data was collected by Reichardt and Bonhoeffer [40] at 313.15 K and 336.15 K, Bloom and Gallup [22] at 298.15 K, and Kuntz and Mains [14] at 298.15 K.

Only two datasets have been reported on the Hg solubility in n-heptane. The first dataset

was reported by Spencer and Voigt [16]. The temperature ranged between 273.15 K and 308.15 K at six isotherms. The second dataset was measured by Okouchi and Sasaki [21] at six isotherms between 278.15 and 313.15 K.

Compared with other aliphatic hydrocarbons, more datasets are available on the Hg solubility in n-octane with broader temperature ranges. The dataset measured by Spencer and Voigt [16] included six isotherms between 273.15 K and 313.15 K. Okouchi and Sasaki [21] also reported the data for six isotherms between 278.15 K and 313.15 K. Bloom and Gallup [25] and Vogel and Gjaldbeak [18] have measured the Hg content at 298.15 K. Marsh et al. [27] conducted the measurements with a broader temperature range between 233.15 K and 413.15 K at five isotherms. Migdisove et al. [23] and Miedanrer et al. [24] conducted Hg solubility measurements at higher temperature conditions. Migdisove et al. [23] measured the Hg solubility between 382.83 K and 482.95 K. Although they conducted repeatability tests at some temperature conditions, the data was quite variable. Miedanrer et al. [24] reported the Hg solubility at three isotherms which were 383.15, 423.15, and 473.15 K.

Regarding decanes, Klehr and Voigt [13] measured the Hg solubility in n-decane between 273.15 K and 318.15 K. Kuntz and Mains [14] also conducted the solubility measurement at 298.15 K. The Hg solubility in dodecane was measured by Bloom and Gallup [22] at 294.65 K and 298.15 K. Miedanrer et al. [24] also measured the Hg solubility at five isotherms between 383.15 K and 498.15 K.

2.4.2 Water

Compared with all other substances investigated in this thesis, many datasets can be found in the literature for the Hg solubility in water. **Figure 2.4** shows the reported Hg solubility in water. These experiments cover a wide range of temperatures between 273.15 K and 780.15 K, at pressure up to 102.3 MPa. Okouchi and Sasaki [22] measured the Hg solubility in water at temperatures between 278.15 K and 313.15 K at atmospheric pressure. Similar measurements were performed by

Onat [19] and Choi and Tuck [15] at temperatures from 298.15 to 363.15 K. Spencer and Voigt [16] were the other researchers who reported measurements of Hg solubility in water. These measurements were conducted at six isotherms with a temperature range of 273.16 to 313.15 K. Glew and Hames [17] measured the equilibrium concentration of Hg in water at various temperatures from 277.45 to 345.59 K. Sanemasa [29] conducted experiments at atmospheric pressure and in a temperature range of 278.15 to 333.15 K. Sorokin et al. [20] measured the Hg solubility high temperature region ranged from 571.15 K to 780.15 K, at pressure up to 102.3 MPa using a reaction vessel made of titanium alloy. Although Sanemasa's measured data was in close agreement with the other researchers in low-temperature region, there are considerable discrepancies between his data measured and the other researchers in the high-temperature region. Clever et al. [41] pointed out that possible air oxidation might have affected the measurements by Sanemasa [29]. Recently, Gallup et al. [26] carried out solubility measurements at atmospheric pressure. The temperature range in their measurements was 273.15 to 373.15 K. The most recent data was reported by Corns et al. [28], and the temperature condition ranged from 41 °F (278.15 K) to 120 °F (322.04 K) at four isotherms. Okouchi and Sasaki [22], Spencer and Voigt [16], Glew and Hames [17], Gallup et al. [26], and Corns et al. [28] added reducing agents, such as tin (II) compounds or hypophosphorous acid to prevent the oxidation of elemental Hg during their experiments.

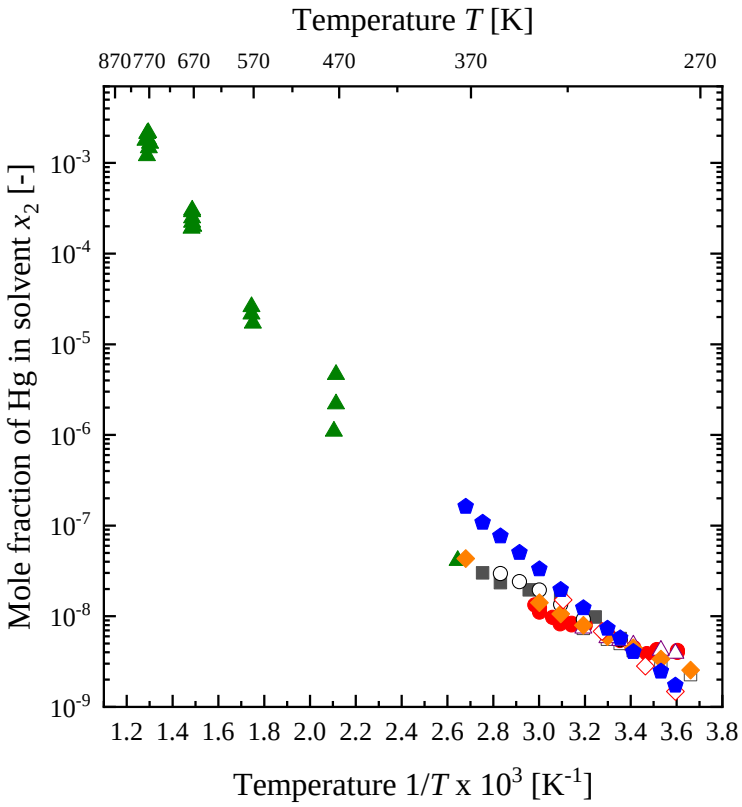

Fig. 2.4 Reported Hg solubility in water: Choi and Tuck [15] (■); Spencer and Voigt [16] (□); Glew and Hames [7] (●); Onat [19] (○); Sorokin et al. [20]: (▲); Okouchi and Sasaki [22] (△); Gallup et al. [26] (◆); Corns et al. [28] (◇); Sanemasa [29] (⬟).

2.4.3 Alcohol

Gallup et al. [26] measured the Hg solubility in methanol, and the temperature ranged between 243.15 K and 373.15 K. Another experimental measurement was conducted by Spencer and Voigt [42] at six isotherms between 298.15 K and 308.15 K. Li et al. [30] also reported the Hg solubility in methanol at five isotherms ranged from 253 to 333 K. The most recent data was reported by Corns et al. [28]. They conducted the measurements for pure methanol and an aqueous solution of methanol, for which concentrations were 90 wt% and 50 wt%. The temperature condition ranged from 41 °F (278.15 K) to 120 °F (322.04 K) for four isotherms. **Figure 2.5** shows the reported Hg solubility in methanol. The Hg concentration increased as a function of increasing temperature and methanol concentration in the aqueous solution.

The investigation of Hg solubility in other alcohols was performed by Spencer and Voigt

[42], Bloom and Gallup [25], and Gallup et al. [26]. The Hg solubility in 1-propanol was investigated at eleven isotherms between 243.15 K and 373.15 K, and Spencer and Voigt [42] investigated the Hg solubility in 2-propanol at five isotherms ranging from 288.15 K to 308.15 K. Similar to the Hg solubility measurement in water, reducing agents were used to prevent the oxidation of elemental Hg in all studies mentioned above.

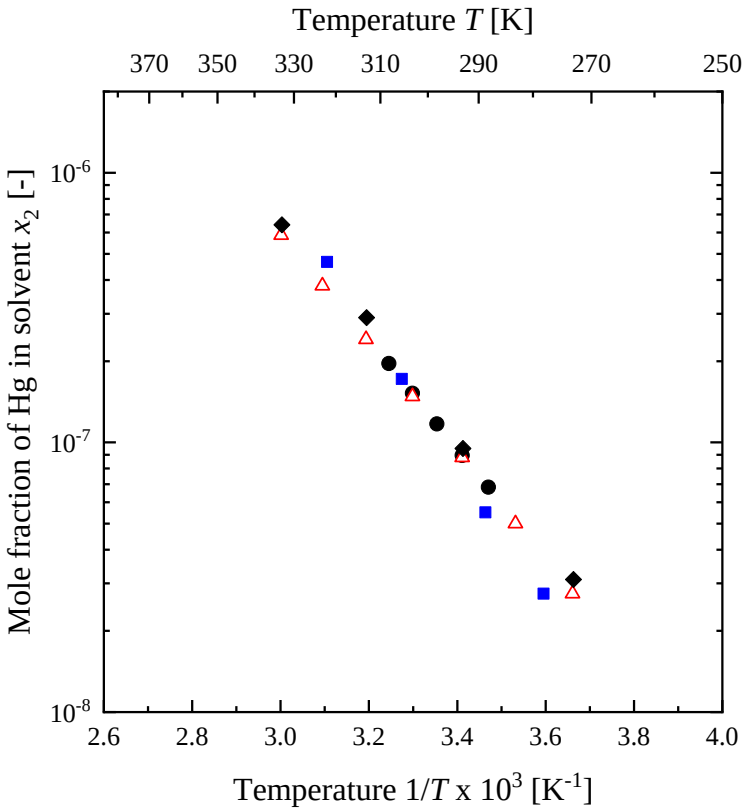

Fig. 2.5 Reported Hg solubility in methanol: Spencer and Voigt [42] (●); Gallup et al. [26] (△); Li et al. [30] (◆); Corns et al. [28] (■).

2.4.4 Glycols

The Hg solubility in glycols has been reported only for MEG and TEG; the Hg solubility in other glycols, such as DEG, has never been reported. Gallup et al. [26] reported the Hg solubility in an aqueous solution of MEG and TEG. The concentrations of MEG solution were 99.1 wt%, 81.6 wt%, and 42.6 wt%, and the temperature condition in each solution was at three isotherms which were 274.65 K, 293.15 K, and 323.15 K. The concentrations of TEG solution were 99.1 wt%, 81.5

wt%, and 42.4 wt%, and the measurement was conducted just at 293.15 K. They used tin (II) citrate as a reducing agent to prevent the oxidation of elemental Hg. Similar measurements were performed by Li et al. [30]. They conducted the Hg solubility measurement for pure MEG and TEG by a closed-loop apparatus with the seven isotherms between 253 K and 373K. They also performed the Hg solubility measurements on the aqueous solution of MEG and TEG. The concentrations of MEG solution were 99 wt%, 82 wt%, and 40 wt%, and the temperature condition was at five isotherms between 253 K and 373 K. The concentrations of TEG solution were 99 wt%, 80 wt%, and 40 wt%, and the temperature condition was at five isotherms between 293 K and 373 K. The most recent data on the Hg solubility in MEG and TEG were reported by Corns et al. [28]. They conducted the Hg solubility measurements in pure MEG and TEG, and the temperature condition ranged from 41 °F (278.15 K) to 120 °F (322.04 K) at four isotherms. They also conducted the measurements for 80 wt% of an aqueous solution of MEG and TEG with the same temperature condition as pure MEG and TEG. They added tin (II) chloride as a reducing agent to prevent the oxidation of elemental Hg. **Figure 2.6** shows the reported Hg solubility in MEG and TEG. The Hg measurements for MEG and TEG by three researchers show a similar tendency in which the Hg concentration increased due to increasing temperature and concentration of glycols in an aqueous solution. Additionally, the Hg solubility in TEG was shown to be greater than in MEG.

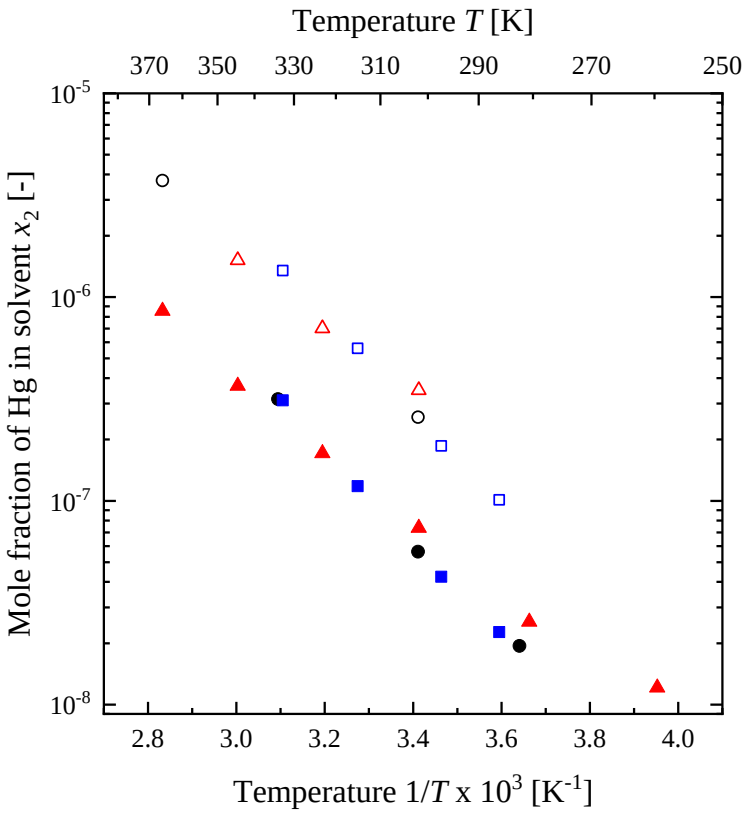

Fig. 2.6 Reported Hg solubility in MEG and TEG: Gallup et al. [26]: MEG: (●); TEG: (○); Li et al. [30]: MEG: (▲); TEG: (△); Corns et al. [28]: MEG: (■); TEG: (□).

2.4.5 Amines

Only Corns et al. [28] reported Hg solubility in aqueous amine solutions. They measured 30 wt% and 15 wt% monoethanolamine (MEA) solutions and 50 wt% and 35 wt% of MDEA solution, with temperature conditions ranging from 41 °F (278.15 K) to 120 °F (322.04 K) at four isotherms. Tin (II) chloride was added as a reducing agent to prevent the oxidation of elemental Hg. The Hg concentration increased due to the increasing temperature and concentration of amines in the aqueous solution.

2.5 Prediction method for Hg solubility in vapor and liquid phase

Several thermodynamic approaches have been used to develop models to predict Hg solubility and distribution. Edmonds et al. [36] first demonstrated a method by using EOS to calculate the solubility of elemental Hg in hydrocarbons and partitioning between gas and condensate phases.

They modified the SRK-EOS and tuned binary interaction parameters using literature data for Hg solubility. They also implemented the prediction model in their commercial simulation software, Multiflash, manufactured by KBC Advanced Technologies plc.

Smit et al. [37] calculated the mercury distribution in natural gas processing facilities using SMIRK-EOS, which contains binary interaction parameters for hydrocarbons, water, and TEG. However, the details of the model were not disclosed. Khalifa and Lue [42] developed a group-contribution method to estimate the binary interaction parameters between mercury and some organic compounds for the SRK-EOS. Koulocheris et al. [39] investigated the PR–EOS with the UNIFAC activity coefficient model (UMR-PRU) to calculate Hg solubility in hydrocarbons, nitrogen, carbon dioxide, water, and methanol. A non-cubic EOS was also investigated by Polishuk et al. [44]. They proposed the Critical Point-based Perturbed-Chain Statistical Association Fluid Theory (CP-PC-SAFT), with which they demonstrated Hg solubility in gaseous and light hydrocarbons by using a universal binary interaction parameter which was $k_{ij} = 0.3$. Although the prediction models suggested by Khalifa and Lue [43] and Koulocheris et al. [39] can estimate binary interaction parameters using group contribution methods for compounds, Hg solubilities are generally not available; therefore, implementation of the models on commercial simulators is complicated. A more simplified prediction model is preferred in practical use, as with the model for the saturated vapor pressure of Hg. The CP-PC-SAFT proposed by Polishuk et al. [44] could predict Hg solubilities in hydrocarbons by using only one binary interaction parameter; however, the applicability of this model to polar compounds such as glycols and amines has not been investigated.

2.6 Overview on measurements and modeling of Hg in vapor and liquid phases

The Hg solubilities in the vapor and liquid phases discussed throughout this section are summarized in **Table 2.1**. Although the Hg solubilities were mainly investigated in liquid hydrocarbons, water, and alcohol, data for solutions in lighter hydrocarbons, such as methane and ethane, and carbon dioxide was minimal. Moreover, the datasets of the Hg solubility in glycols and

amines were also extremely few or not available in public. VLE and LLE data are essential for tuning the prediction model for Hg distribution in natural gas processing facilities.

Regarding methods for Hg solubility measurement in the vapor phase, Butala et al. [11] first developed the apparatus based on the flow method. Chapoy et al. [12] also used a similar flow-type apparatus to Butala et al. However, contact methods between Hg and gases in the saturation cell were not mentioned in their literature. Regarding methods for Hg solubility measurement in the liquid phase, a static method was widely employed. Additionally, Gallup et al. [25] found a significant deviation between total Hg and elemental Hg concentration in oxygen-containing solvents, such as alcohols, without reducing agents and copper fillings during the solubility measurements for elemental Hg. They suggested that the deviation indicated the presence of ionic Hg (Hg^{2+}), caused by the oxidation of elemental Hg, because the solubility of $HgCl_2$ in hydrocarbons and alcohols was significantly greater than that of elemental Hg [25]. To avoid the enhancement of Hg solubility, Gallup et al. and some researchers added a small amount of reducing agents to solvents to prevent the oxidation of elemental Hg. Li et al. [30] constructed the closed-loop apparatus.

Regarding prediction methods, a modified version of the Wagner equation and the simplified Antoine equation were proposed to calculate the saturated vapor pressure of Hg. The Wagner equation is based on the principle of corresponding states, allowing it to be applied to pure components. However, the application of the Wagner equation to the mixture is complex. Cubic EOS approaches were widely used to predict the Hg solubility in the vapor and liquid phase. Although calculating the LLE by cubic EOS is not common, it can be applied to calculate the Hg solubility in the liquid phase. Group contribution methods to estimate binary interaction parameters and the PC-SAFT were also suggested; however, simplified prediction methods are preferred given the practical use of commercial simulators.

Table 2.1. Availability of Hg solubility dataset

System	Type of equilibrium	Temperature [K]	Pressure [MPa]	References
Methane	VLE	244 – 323	0.80 – 18.6	11, 12
Ethane	VLE/LLE	244 – 323	0.70 – 11.4	12, 39
Propane	VLE	247 – 529	1.03 – 3.45	10, 11, 12
Butane	VLE/LLE	263 – 573	0.001 – 38.5	9, 10, 11
Pentanes	LLE	233 – 383	Ambient – 2.06	11, 14, 21, 25, 26
Hexanes	LLE	273 – 336	Ambient	14, 16, 21, 22, 40
Heptanes	LLE	273 – 313	Ambient	16, 21
Octanes	LLE	273 – 483	Ambient	16, 18, 21, 23, 24, 25, 27
Decanes	LLE	273 – 318	Ambient	13, 14
Dodecanes	LLE	295 – 498	Ambient	22, 24
Carbon dioxide	VLE	234 – 323	0.39 – 13.8	11, 12
Nitrogen	VLE	244 – 323	0.70 – 17.3	12, 36
Water	LLE	273 – 780	Ambient – 102	15, 16, 17, 19, 20, 22, 26, 28, 29
Alcohols	LLE	243 – 373	Ambient	25, 26, 28, 30, 42
Glycols	LLE	253 – 373	Ambient	26, 28, 30
Amines	LLE	278 – 322	Ambient	28

VLE: vapor-liquid equilibrium

LLE: liquid-liquid equilibrium

Chapter 3 Experimental Section

3.1 System investigated

In this thesis, the following experiments were carried out:

I. Investigation of VLE of Hg

1) *Measurement of saturated vapor pressure of Hg*

The saturated vapor pressure of Hg was measured from 278.15 K to 298.15 K to ensure the reliability of the experimental data.

2) *Measurement of Hg solubility in compressed methane, ethane, carbon dioxide, and artificial natural gas*

Hg solubility in methane, ethane, carbon dioxide, and an artificial natural gas composed of methane, ethane and carbon dioxide was measured at high pressures. The temperature range was set from 268 K to 303 K, and the pressure from 0.5 MPa to 6.0 MPa.

II. Investigation of LLE of Hg

1) *Measurement of Hg solubility in methanol*

Hg solubility in methanol was measured under the atmospheric pressure at 303 K to 333 K to ensure the reliability of the experimental data.

2) *Measurement of Hg solubility in solvents for natural gas processing*

Hg solubility in five solvents for natural gas processing were measured under atmospheric pressure, with the temperature range set from 303 K to 333 K. These solvents included: methanol, MEG, DEG, TEG, and MDEA.

3.2 Materials

Table 3.1 lists the sample gas and the chemicals used in this study. Except for the artificial natural gas, the supplier reported purities are used. All sample gases and chemicals were used as received without further purification. Highly purified gases were purchased from suppliers especially for nitrogen and methane. Comparing with the two gases, the purities of ethane and carbon dioxide

were slightly low, 99.95 vol.% and 99.99 vol.%, respectively. Some researchers pointed out that water, as an impurity in carbon dioxide, sometimes affected its phase behavior. The discussion will be described later. However, ethane and carbon dioxide were used as highest as purities we could purchased from suppliers. A supplier specially prepared the artificial natural gas for this study. The contents were in the footnote of **Table 3.1**. The balance gas was methane, and the other components were ethane and carbon dioxide. However, as the five solvents, methanol, MEG, DEG, TEG, and MDEA, have some hygroscopicity, the density was measured by an oscillating U-tube density meter (Anton-Paar, Graz, Austria, DMA 5000M) at 298.15 K.

Table 3.2 compares the literature data at 298.15 K [45, 46]. The experimental data was within 0.17% of the literature values. Although mixing with water usually increases solvent density because of the difference in molecular size of water and solvents, it decreases solvent density in some cases when there is a strong interaction between water and solvents molecules, such as in icebergs. However, the lower density of MEG, DEG, and MDEA in measured data than that of literature data may have been caused by water mixing, though the gap between the measured data and literature data was not significantly different, and there may be no such influence on the measured density of methanol and TEG.

Table 3.1. Chemical reagent and sample gases employed in this study

	Molecular weight M_w	CAS RN	Supplier	Grade	Purity
Mercury	[a]200.5920	7439-97-6	Kanto Chemical, Tokyo	Special	99.5 mass %
Nitrogen	28.01	7727-37-9	Taiyo Nippon Sanso, Tokyo	Grade 1	99.99995 vol.%
Methane	[b]16.043	74-82-8	Tokyo Gas Chemicals, Tokyo	5N5 Grade	99.9995 vol%
Ethane	[b]30.070	74-84-0	Tokyo Gas Chemicals, Tokyo	Research Grade	99.95 vol.%
Carbon dioxide	[b]44.010	124-38-9	Showa Denko Gas Products, Kawasaki, Japan	4N grade	99.99 vol%
[c]Artificial natural gas	[e]18.46	-	Takachiho Chemical Industrial, Tokyo	[c]Prepared for this study	-
Methanol	[e]32,042	67-56-1	Kanto Chemical, Tokyo	Special	99.98 mass%
MEG	[e]62.068	107-21-1	Kanto Chemical, Tokyo	Special	99.5 mass %
DEG	[e]106.122	111-46-6	Kanto Chemical, Tokyo	[f]RoHs2	99.5 mass %
TEG	[e]150.175	112-27-6	Tokyo Chemical Industry, Tokyo	Special	99.0 mass%
MDEA	[e]105.137	105-59-9	Tokyo Chemical Industry, Tokyo	Chemical	99.0 mass %

[a]Reported by supplier

[b]Ref. [47]

[c]Methane based, Ethane 5.10 vol. %, Carbon dioxide 6.10 vol. %

[d]Calculated from molecular weight of 16.043 (methane), 30.070 (ethane), 44.010 (carbon dioxide) [47]

[e]Ref. [48]

[f]Acceptable chemical for the Restriction of the use of certain Hazardous Substances ver. 2

Table 3.2. **Liquid density of chemical reagent**

	Density at 298.15 K [kg· m^{-3}]		Relative error [%]	Ref.
	This work ρ	Literature ρ_{lit}		
Methanol	786.63	786.37	0.0331	45
MEG	1109.85	1110.00	-0.0135	45
DEG	1112.83	1116.54	-0.332	45
TEG	1119.92	1119.50	0.0375	45
MDEA	1035.63	1037.40	-0.171	46

3.3 Apparatus

3.3.1 Apparatus for measurements of vapor-liquid equilibrium of Hg in compressed gases

Figure 3.1 shows a schematic diagram of the apparatus. The apparatus was based on a flow method, and the main piping and assemblies were put in a constant temperature bath (Thomas Ltd., Tokyo, TRL-101FEZ) with an inner volume of 32 L. The equilibrium cell was a sample tube made of stainless steel 316 (Swagelok Co., Solon, U.S., SS-4CS-TW-25) with an inner volume of 25 cm^3. A cross-sectional view of the cell is shown in the figure. Spherical packings, made of tungsten carbide with o.d. 3 mm, were installed into the cell. The elemental Hg was loaded into the cell, and the sample gas was introduced into the cell. As described in **section 3.2**, water dissolved in carbon dioxide sometimes affects its phase equilibrium. A gas dryer should be installed downstream of the gas regulator. However, since the depressurized carbon dioxide was directly introduced into the heat changer, the gas seemed be distilled during measurements and be in a higher purity of the gas sample. The flow rate and the sample gas pressure were controlled with a needle valve (Swagelok Co., Solon, U.S., SS-0RS2).

After saturating with Hg vapor, the sample gas was depressurized to the atmospheric pressure by the needle valve. Then, the gas was mixed with a nitrogen flow from a digital mass flow controller (Azbil Co., Tokyo, MQV0050). The Hg concentration in the gaseous phase was

continuously measured by a portable mercury survey meter (Nippon Instruments Co., Tokyo, EMP-2) based on the CVAAS with an analytical wavelength of 253.7 nm. The detection range of the Hg concentration was up to 999.9 μg· Nm^{-3}. The measured Hg concentration was converted to the mole fraction of Hg by using the sample gas and nitrogen flow rates. The precise flow rate was measured using a wet gas meter (Shinagawa Co., Tokyo, W-NK-0.5) with a minimum indicator volume of 1 cm^3. The experimental temperature was measured with a built-in Pt resistance thermometer in the constant temperature bath. The pressure was determined using the averaged value from two pressure transducers (Kyowa Electronic Instruments Co., Tokyo, PG-100KU and PHB-A-10MP) set at the inlet and outlet of the cell. The maximum capacity of these transducers was 10 MPa. After analysis of the Hg concentration, the gas was finally sent to a column packed with a metal sulfide adsorbent for Hg removal and then diffused into the air. In the measurements, the estimated uncertainty of the temperature T, the gauge pressure P_g and the Hg concentration $C_{Hg,\,sensor}$ were $u\,(T)$ = 0.05 K, $u\,(P_g)$ = 0.003 MPa, and $u\,(C_{Hg,\,sensor})$ = 0.4 μg· Nm^{-3}, respectively.

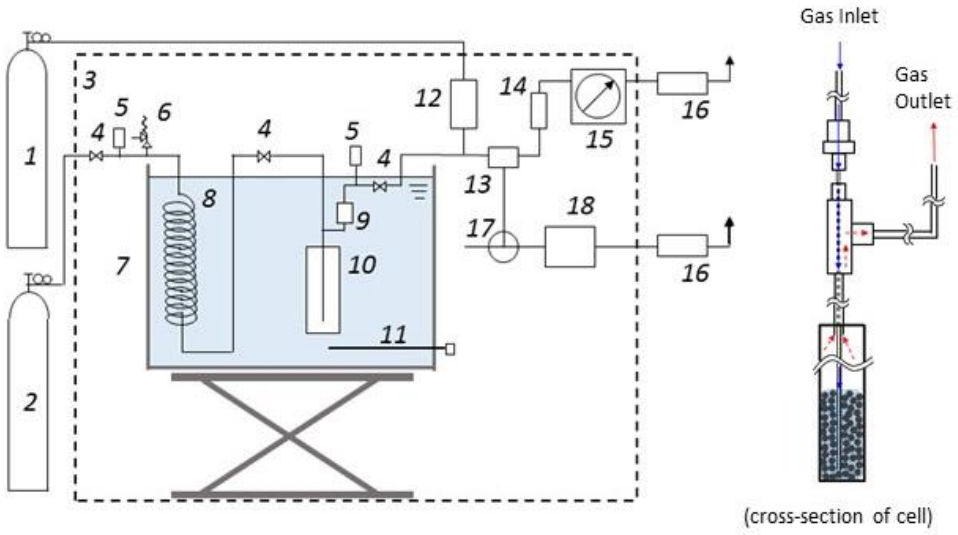

Fig. 3.1. Schematic diagram of apparatus for Hg solubility measurements in high pressure gas; 1: Nitrogen cylinder 2: Sample gas cylinder 3: Air chamber 4: Needle valve 5: Pressure gauge 6: Relief valve 7: Constant temperature bath 8: Heat exchanger 9: In-line filter 10: Equilibrium cell 11: Built-in Pt resistance thermometer 12: Mass flow controller 13: Sampling port 14: Rotor meter 15: Wet gas meter 16: Absorber column for Hg 17: three-way valve 18: Mercury survey meter

The uncertainty of the mole fraction of Hg in the sample gas u (y_2) and that of the pressure u (P) is described later. Effective digits of y_2 depend on u (y_2) because it was evaluated not only from T, P_g and $C_{\mathrm{Hg,\ sensor}}$ but also from flow rate of sample gases and nitrogen.

3.3.2 Apparatus for measurements of liquid-liquid equilibrium of Hg in solvents

Figure 3.2 indicates a schematic of the experimental apparatus. The apparatus was based on a static method and constructed in this research. All solvents, methanol, MEG, DEG, TEG, and MDEA, were well purged with nitrogen gas before the experiment. Next, 40 mL of solvent was poured into borosilicate amber vials, successively and approximately 150 μL of liquid elemental Hg was put into the vials. In this way, elemental Hg was introduced into the organic liquid phase. After sealing tightly with a screw cap under a nitrogen atmosphere, the sample vials were placed in a constant-temperature dry bath (Taitec Corporation, Saitama, Japan, DTU-2CN) and allowed to settle for about two weeks until attaining equilibrium. The temperature range of the experiments was 298 K to 333 K. A sample vial without Hg was separately prepared as a reference for the temperature of the samples. A small hole was bored through the screw cap to insert a thermistor thermometer (T&D Corporation, Nagano, Japan, TR-1320). The reference temperature was measured using the thermometer and assumed to be the same as the temperature of the samples. Aliquots of samples for analysis were periodically taken from the organic phase in the sample vials and were transferred to analytical vials at room temperature. The analytical vials were filled with the same solvent as the samples beforehand to avoid precipitation of elemental Hg.

The experimental procedures mentioned above were conducted in a nitrogen-purged glove box (UNICO, Ibaraki, Japan, UL-800A). The Hg concentration in the samples was analyzed by a total Hg analyzer (Nippon Instruments, Tokyo, MA-3000) based on the CVAAS. The calibration curve was prepared by the standard solution made from 100 mg· L^{-1} of mercury chloride solution (FUJIFILM Wako Pure Chemical Corporation, Osaka, Japan) with L-cystine solution (Kanto Chemical, Tokyo) as a diluent reagent. The measured Hg concentration was converted to the mole

fraction of Hg in the solvents considering the sampling and dilution conditions. The uncertainties for the temperature T and the amount of Hg $m_{Hg,app}$ detected by the total Hg analyzer were estimated to be u (T) = 0.6 K and u ($m_{Hg,app}$) = 0.003 ng, respectively. The uncertainty of the mole fraction of Hg in the solvents, $u(x_2)$, will be described later. Effective digits of x_2 depend on u (x_2) because it was evaluated not only from T and $m_{Hg,\ app}$ but also from statistical dispersion of x_2.

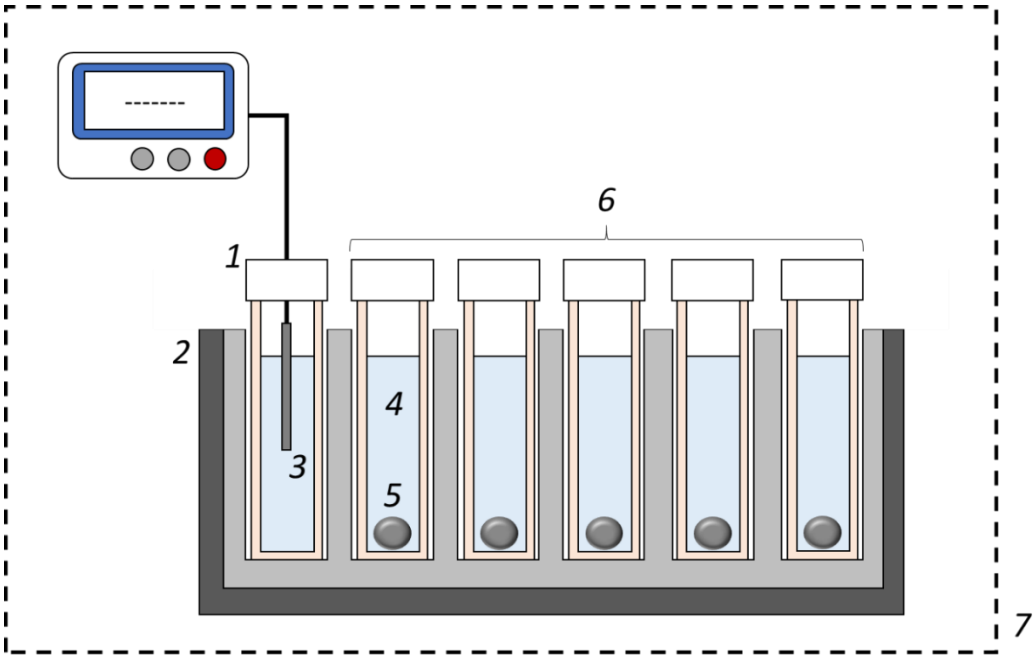

Fig. 3.2. Schematic of experimental apparatus for Hg solubility measurements in solvents; 1: Reference vial for temperature measurement, 2: Constant-temperature dry bath, 3: Thermistor thermometer, 4: Solvent, 5: Elemental Hg, 6: Sample vials, 7: Nitrogen purged glove box.

3.4 Data correlation and prediction

3.4.1 Equation of state

The experimental data of vapor-liquid and liquid-liquid equilibrium of Hg in substances were correlated with the PR-EOS [47]:

$$P = \frac{RT}{v-b} - \frac{a}{v^2 + 2bv - b^2} \tag{1}$$

where the attractive parameter a and the excluded volume parameter b were evaluated from the critical temperature T_c, critical pressure P_c, and acentric factor ω:

$$a = 0.45724 \frac{R^2 T_c^{\,2}}{P_c} \alpha \tag{2}$$

$$b = 0.07780 \frac{R T_c}{P_c} \tag{3}$$

$$\alpha = \left[1 + \kappa \left\{ 1 - \left(\frac{T}{T_c} \right)^{1/2} \right\} \right]^2 \tag{4}$$

$$\kappa = 0.37464 + 1.5226\omega - 0.266992\omega^2 \tag{5}$$

The critical temperature and pressure of Hg obtained from the literature [31, 32] were used for the attractive parameter. The temperature dependence of the attractive parameter for Hg is described later. As literature values of the acentric factor of Hg were very few, it was estimated from the definition of the acentric factor [47] and the empirical equation for saturated Hg vapor pressure, P_2^S [31, 32]:

$$\omega = -\log_{10} \frac{P_2^{\,s}}{P_{c,2}}\bigg|_{\frac{T}{T_{c,2}}=0.7} - 1.000 \tag{6}$$

$$\ln\left(\frac{P_2^{\,s}}{P_{c,2}} \right) = \left(\frac{T_{c,2}}{T} \right) \left(a_1 \tau + a_2 \tau^{1.89} + a_3 \tau^2 + a_4 \tau^8 + a_5 \tau^{8.5} + a_6 \tau^9 \right) \tag{7}$$

$$\tau = 1 - \frac{T}{T_{c,2}} \tag{8}$$

where $P_{c,2}$ and $T_{c,2}$ are the critical pressure and critical temperature of Hg, respectively.

The attractive parameters of methane, ethane, carbon dioxide, and methanol were calculated with a modified version of the PR–EOS by Stryjek and Vera (PRSV-EOS) [50]. In the PRSV-EOS, the constant values in the attractive parameter and the excluded volume parameter were slightly different from those in **Eqs. (2)** and **(3)**. A new parameter κ_1 was introduced to calculate the saturated vapor pressure precisely.

$$a = 0.457235 \frac{R^2 T_c^{\,2}}{P_c} \alpha \tag{9}$$

$$b = 0.077796 \frac{R T_c}{P_c} \tag{10}$$

$$\kappa = \kappa_0 + \kappa_1 \left\{ 1 + \left(\frac{T}{T_c} \right)^{1/2} \right\} \left(0.7 - \frac{T}{T_c} \right) \tag{11}$$

$$\kappa = 0.378893 + 1.4897153\omega - 0.17131848\omega^2 + 0.0196554\omega^2 \tag{12}$$

where the value of κ_1 was obtained from the literature [50]. **Table 3.3** lists the parameter for **Eqs. (2) to (10)**.

Table 3.3. Parameters used to estimate constants in PR/PRSV-EOS

	Critical temperature T_c [K]	Critical pressure P_c [MPa]	Acentric factor ω [-]	Parameter in PRSV-EOS κ_1 [-]
Mercury	[a]1764	[a]167	[b]-0.190	-
[c]Methane	190.555	4.505	0.01045	0.00159
[c]Ethane	305.43	4.87976	0.09781	0.02669
[c]Carbon dioxide	304.21	7.38243	0.22500	-0.04285
[c]Methanol	512.58	8.09579	0.56533	-0.16816
[d]MEG	720.00	8.20	0.514	
[d]DEG	750.00	4.80	0.580	
[d]TEG	790.00	3.45	0.782	
[e]MDEA	678.00	3.88	1.302	

[a]Refs. [31] [32]

[b]discussed in Chapter 4.1.3

[c]Ref. [50]

[d]Ref. [51]

[e]Ref. [48]

A conventional function based on the van der Waals one-fluid model was used as the mixing rule for **Eq. (1)**:

$$a = \sum_i \sum_j x_i x_j (1 - k_{ij})(a_i a_j)^{1/2} \tag{13}$$

$$b = \sum_i \sum_j x_i x_j \frac{b_i + b_i}{2} \tag{14}$$

where k_{ij} (= k_{ji}) is the binary interaction parameter. It is known to have temperature dependences. In this research, the following function, which is generally used in commercial process simulators, such as Aspen Plus, was adopted:

$$k_{ij} = k_{ij}^0 + k_{ij}^1 T + \frac{k_{ij}^2}{T} \tag{15}$$

where *i* and *j* are cumulative in the three coefficients k_{ij}^0, k_{ij}^1 and k_{ij}^2.The values are determined using the experimental data to minimize the objective function. The selection of the objective function will be described later.

3.4.2 Calculation of saturated vapor pressure of Hg

When Hg in the vapor phase becomes the saturation condition, the fugacity of Hg in the vapor phase equals the liquid Hg phase:

$$f_1^V = f_1^L \tag{16}$$

The PR-EOS calculates the fugacity of Hg in the vapor phase, f_1^V. The fugacity of the liquid Hg phase was calculated as that of the solid elemental Hg under the assumption that the elemental Hg phase was a liquid without immiscibility or a solid with fluidity:

$$f_i^L = P_i^s \exp\left[\frac{v_i^s (P - P_i^s)}{RT}\right] \tag{17}$$

where P_i^s and v_i^s are the saturated vapor pressure and the saturated molar volume of elemental Hg, respectively.

3.4.3 Calculation of phase equilibrium

For vapor-liquid equilibrium of Hg in pure gases, components 1 and 2 correspond to the pure gas and elemental Hg, respectively. Therefore, elemental Hg is just in the vapor and liquid phase. The equilibrium condition is given by:

$$f_2^V = f_2^L \tag{18}$$

where f_2^V is the fugacity of Hg in the vapor phase calculated by the PR-EOS, and f_2^L is the fugacity of Hg in the liquid Hg phase, calculated by **Eq. (17)**.

For vapor-liquid equilibrium of Hg in the artificial natural gas, components 1, 2, 3, and 4 correspond to methane, ethane, carbon dioxide, and elemental Hg, respectively. The equilibrium condition is given in the same manner as the vapor-liquid equilibrium of Hg in pure gases:

$$f_4^V = f_4^L \tag{19}$$

For liquid-liquid equilibrium of Hg in solvents, components 1 and 2 correspond to the solvent and elemental Hg, respectively. Therefore, the solvent is in the vapor and liquid phases. Elemental Hg is in the vapor and two liquid phases. So, the equilibrium condition is given by **Eq. (16)** and the following equation:

$$f_2^V = f_2^L = f_2^{L2} \tag{20}$$

where f_2^{L2} is the fugacity of Hg in the liquid Hg phase calculated by **Eq. (17)**. The detail of the calculation is described in the later section.

Chapter 4 Vapor-Liquid Equilibrium of Hg in compressed gases

4.1 Vapor-liquid equilibrium of Hg in pure gases

4.1.1 Measurement of saturated vapor pressure of Hg

The saturated vapor pressure of Hg was measured at 278.15 to 298.15 K to verify the reliability of the apparatus. **Fig. 4.1** shows the saturated vapor pressure of Hg, and **Table 4.1** lists the experimental data. The saturated vapor pressure was measured in the nitrogen flow from 0.40 to 0.46 L· min^{-1} under atmospheric pressure. The Hg saturated gas flowing from the equilibrium cell was diluted by the nitrogen upstream of the mercury survey meter, which did not exceed its maximum detection range of 999 μg· Nm^{-3}. These results represent Hg solubility in nitrogen. According to previous research, the partial pressure of Hg should increase by ~0.1% for a nitrogen density of 10 mol· L^{-1} at 323 K [41]; the nitrogen density has been estimated to be around 0.04 mol· L^{-1} [52] under the experimental condition. Therefore, it does not affect the experimental vapor pressure of mercury. Ernsbeger and Pitman [53], Hildenbrand et al. [54], and Hill [55] have reported the saturated Hg vapor pressure at 285.22 K to 326.63 K, 295.0 K to 331.6 K, and 272.45 K to 308.03 K, respectively. The saturated vapor pressure of Hg was estimated using **Eqs. (7) and (8)**; the calculation was also shown in **Fig. 4.1**. As shown in **Table 4.1**, the saturated vapor pressure ranged from 0.05 to 0.3 Pa in the experimental temperature range. Although the experimental data showed a tendency similar to that of the data obtained by Hildebrand et al. [54], the data was slightly higher than those obtained by Ernsbeger and Pitman [53]. **Fig. 4.2** shows the van't Hoff plot of the saturated vapor pressure of Hg. The experimental data were correlated with the van't Hoff equation:

$$\ln P_2^S - \ln P_{2,298.15K}^S = -\frac{\Delta H_{vap}}{R}\left(\frac{1}{T} - \frac{1}{298.15}\right) \tag{21}$$

where $P_{2,298.15K}^S$ and ΔH_{vap} are the vapor pressure at a reference temperature, 298.15 K and the vaporization enthalpy of Hg, respectively. The value of ΔH_{vap} was 62.90 kJ· mol^{-1}.

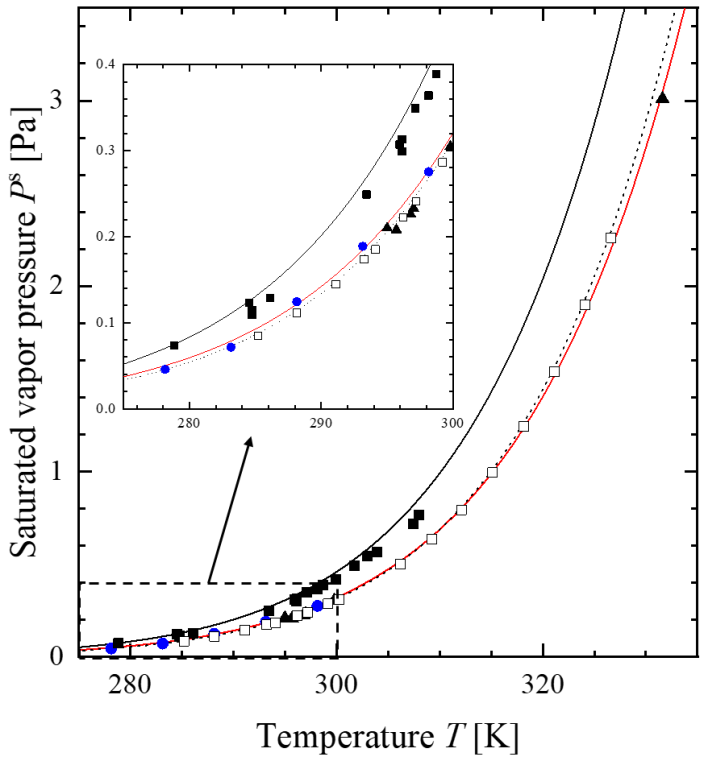

Fig. 4.1. Saturated vapor pressure of Hg: this work (●); Ernsberger and Pitman [53] (□); Hildenbrand at al. [54] (▲); Hill [55] (■); PR-EOS (——); Eq. (7) (·····); PR-EOS with Eq. (17) (——).

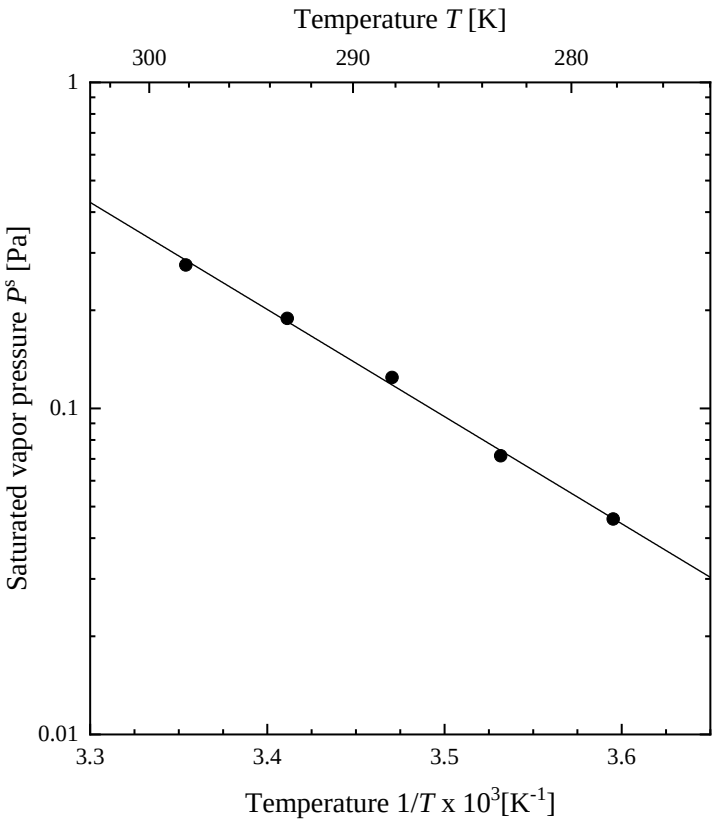

Fig. 4.2. The van't Hoff plot of saturated vapor pressure of Hg.

Table 4.1. Saturated vapor pressure of Hg

[a]Temperature	Saturated vapor pressure of Hg	
T [K]	$P_2^s \times 10^2$ [Pa]	$u\,(P_2^s) \times 10^2$ [Pa]
278.15	4.579	0.012
283.15	7.154	0.026
288.15	12.44	0.18
293.15	18.88	0.76
298.15	27.53	0.55

[a]$u\,(T) = 0.05$ K

4.1.2 Measurement of Hg solubility in pure gases

Table 4.2 lists the experimental data of Hg solubility in methane, and **Fig. 4.3** shows its eight isotherms. The Hg solubility in methane has been reported by Butala et al. [11] for 2.758 MPa, 3.447 MPa, and 6.895 MPa at temperatures from 253.15 K to 293.15 K. Chapoy et al. [12] reported values for pressures of 0.80 MPa to 18.62 MPa and temperatures from 265.15 K to 323.15 K. These are also shown in **Fig. 4.3**. Although the experimental values were slightly lower than those of the literature, the isotherm showed a similar pressure dependence. Therefore, the mole fraction of Hg in the vapor phase decreased with rising pressure and seemed to be a constant or minimum. The latter is sometimes observed in solid-vapor equilibrium (SVE), such as in systems consisting of a solid organic compound in a supercritical fluid [56]. The physical properties of elemental Hg seem similar to organic solids because of their very low miscibility. Although elemental Hg was recognized as the liquid phase, its solubility was similar to that of solid organic compounds in SVE.

Tables 4.3 and **4.4** list the experimental data for Hg solubility in ethane and carbon dioxide, then **Figs. 4.4** and **4.5** show their eight isotherms, respectively. The experimental temperature and pressure range are similar to those for methane. Additionally, the data point for ethane at 300.65 K is not shown in the figure. The Hg solubility in ethane has been reported by Chapoy et al. [12] for 0.83 MPa to 11.38 MPa, and 244.10 K to 323.15 K. Their data on Hg solubility in the vapor phase are

shown in **Fig. 4.4**. The Hg solubility in carbon dioxide has been reported by Butala et al. [11] for 3.475 to 5.702 MPa and 273.15 to 293.15 K, and by Chapoy et al. [12] for 0.39 to 13.794 MPa and 243.15 to 323.15 K. Their data of Hg solubility in vapor phase are shown in **Fig. 4.5**. The pressure dependences were similar to those of methane, and the Hg solubility decreases with increasing pressure.

Table 4.2. Hg solubility in methane

[a]Temperature T [K]	Pressure		Measurement: Mole fraction of Hg		Calculation: Mole fraction of Hg	[b]ARLD
	P [MPa]	u (P) [MPa]	$y_2 \times 10^9$ [-]	u (y_2) $\times 10^9$ [-]	$y_2 \times 10^9$ [-]	$\lvert\Delta \log_{10} y_2\rvert$ [-]
268.15	6.031	0.020	4.842	0.104	4.187	0.00760
273.15	6.042	0.023	7.486	0.072	6.905	0.00432
278.15	6.039	0.031	11.81	0.104	11.18	0.00303
283.15	6.025	0.029	18.40	0.20	17.77	0.00197
288.15	6.029	0.024	27.82	0.17	27.69	0.000273
293.15	6.026	0.021	42.20	0.26	42.47	0.000374
298.15	6.028	0.028	62.87	0.65	65.55	0.00252
303.15	6.030	0.028	91.06	0.43	95.30	0.00280
268.15	3.502	0.014	6.220	0.049	6.315	0.00080
273.15	3.501	0.016	10.21	0.10	10.36	0.00081
278.15	3.486	0.035	15.63	0.23	16.74	0.00382
283.15	3.509	0.026	25.18	0.26	26.33	0.00256
288.15	3.493	0.009	39.14	0.08	41.09	0.00284
293.15	3.497	0.016	59.96	0.33	62.80	0.00279
298.15	3.499	0.010	91.40	0.42	95.83	0.00292
303.15	3.502	0.019	139.4	5.1	140.5	0.000487
268.15	2.816	0.014	7.337	0.138	7.590	0.00181
273.15	2.818	0.014	12.03	0.14	12.42	0.00177
278.15	2.814	0.011	18.77	0.07	20.00	0.00355
283.15	2.814	0.011	29.68	0.10	31.58	0.00358
288.15	2.819	0.010	46.18	0.33	48.97	0.00348
293.15	2.816	0.012	70.43	0.38	74.94	0.00377
298.15	2.801	0.008	107.1	0.6	114.5	0.00419
303.15	2.819	0.012	162.5	5.5	167.5	0.00194
268.15	2.520	0.040	7.821	0.133	8.360	0.00357
273.15	2.526	0.043	12.63	0.20	13.65	0.00428
278.15	2.520	0.035	20.26	0.29	21.98	0.00459

Continued on next page

Table 4.2. Continued from the previous page.

[a]Temperature T [K]	Pressure		Measurement		Calculation	[b]ARLD
			Mole fraction of Hg		Mole fraction of Hg	
	P [MPa]	u (P) [MPa]	$y_2 \times 10^9$ [-]	u (y_2) $\times 10^9$ [-]	$y_2 \times 10^9$ [-]	$\lvert\Delta\log_{10} y_2\rvert$ [-]
283.15	2.525	0.030	31.92	0.39	34.63	0.00472
288.15	2.520	0.034	50.54	0.68	53.86	0.00378
293.15	2.528	0.030	76.87	0.87	82.09	0.00401
298.15	2.540	0.025	117.3	0.4	124.3	0.00362
303.15	2.536	0.028	177.6	6.6	183.1	0.00196
268.15	1.529	0.0365	11.81	0.26	13.14	0.00585
273.15	1.528	0.036	19.37	0.42	21.46	0.00577
278.15	1.539	0.031	31.32	0.55	34.17	0.00504
283.15	1.536	0.023	50.09	0.80	53.94	0.00440
288.15	1.536	0.024	77.65	1.26	83.62	0.00452
293.15	1.540	0.020	125.1	5.1	127.4	0.00112
298.15	1.543	0.026	176.1	6.2	192.3	0.00567
303.15	1.541	0.023	283.6	10.1	284.2	0.000136
268.15	0.552	0.018	31.73	1.31	34.79	0.00533
273.15	0.553	0.011	52.25	1.25	56.53	0.00470
278.15	0.545	0.018	86.18	3.72	91.70	0.00382
283.15	0.549	0.014	142.4	6.6	143.2	0.000355
288.15	0.560	0.019	225.0	9.9	217.4	0.00223
293.15	0.560	0.018	347.7	11.3	331.5	0.00320
298.15	0.552	0.016	544.3	20.5	506.3	0.00501
303.15	0.554	0.022	810.3	38.4	746.7	0.00583

[a]u (T) = 0.05 K

[b]ARLD: absolute relative logarithmic deviation

Table 4.3. Hg solubility in ethane

[a]Temperature T [K]	Pressure		Measured		Calculation	
			Mole fraction of Hg		Mole fraction of Hg	[c]ARLD
	P [MPa]	u (P) [MPa]	$y_2 \times 10^9$ [-]	u (y_2) $\times 10^9$ [-]	$y_2 \times 10^9$ [-]	$\lvert\Delta \log_{10} y_2\rvert$ [-]
298.15	3.516	0.024	104.9	4.1	102.9	0.00121
[b]300.65	3.531	0.034	123.6	5.4	151.6	0.0129
303.15	3.533	0.027	146.4	5.3	150.7	0.00185
278.15	2.548	0.038	21.86	0.36	21.39	0.00124
283.15	2.552	0.031	34.38	0.26	34.96	0.000981
288.15	2.534	0.030	53.56	0.82	55.77	0.00242
293.15	2.547	0.040	83.17	1.40	85.73	0.001861
298.15	2.549	0.021	135.7	4.8	129.1	0.00315
303.15	2.554	0.025	196.6	7.3	190.2	0.00215
268.15	1.581	0.035	11.81	0.14	11.87	0.000292
273.15	1.564	0.023	19.85	0.26	20.32	0.00131
278.15	1.550	0.032	32.51	0.71	33.71	0.00210
283.15	1.560	0.025	51.10	0.65	53.72	0.00298
288.15	1.558	0.031	79.18	1.27	55.77	0.00242
293.15	1.557	0.017	130.5	4.9	129.4	0.000557
298.15	1.558	0.031	199.6	13.0	194.5	0.00166
303.15	1.544	0.019	303.4	10.9	289.9	0.00303
268.15	0.560	0.018	32.44	2.42	33.60	0.00204
273.15	0.556	0.022	55.05	4.41	55.68	0.000682
278.15	0.552	0.024	87.45	7.58	90.38	0.00203
283.15	0.556	0.017	145.9	6.73	141.9	0.00176
288.15	0.554	0.016	240.0	10.2	221.1	0.00537
293.15	0.556	0.013	381.3	13.0	336.5	0.00846

Continued on next page

Table 4.3. Continued from the previous page.

[a]Temperature	Pressure		Measured		Calculation	
			Mole fraction of Hg		Mole fraction of Hg	[c]ARLD
T [K]	P [MPa]	u (P) [MPa]	$y_2 \times 10^9$ [-]	u (y_2) $\times 10^9$ [-]	$y_2 \times 10^9$ [-]	$\lvert\Delta \log_{10} y_2\rvert$ [-]
298.15	0.560	0.014	568.4	20.0	502.3	0.00859
303.15	0.548	0.011	869.3	25.1	759.6	0.00967

[a] u (T) = 0.05 K

[b] Not shown in Fig. 4.4

[c] ARLD: absolute relative logarithmic deviation

Table 4.4. Hg solubility in carbon dioxide

[a]Temperature T [K]	Pressure		Measured		Calculation	
			Mole fraction of Hg		Mole fraction of Hg	[b]ARLD
	P [MPa]	u (P) [MPa]	$y_2 \times 10^9$ [-]	u (y_2) $\times 10^9$ [-]	$y_2 \times 10^9$ [-]	$\lvert\Delta \log_{10} y_2\rvert$ [-]
268.15	2.070	0.034	8.864	0.138	9.258	0.00234
273.15	2.057	0.025	15.20	0.20	15.47	0.000985
278.15	2.045	0.026	25.29	0.52	25.31	0.0000486
283.15	2.057	0.027	39.33	0.47	40.18	0.00125
288.15	2.049	0.016	62.64	0.65	63.21	0.000543
293.15	2.041	0.027	93.63	2.20	97.76	0.00267
298.15	2.029	0.023	143.6	1.4	149.1	0.00238
303.15	2.040	0.023	220.7	5.0	221.8	0.000317
268.15	1.560	0.019	11.88	0.17	12.24	0.00164
273.15	1.555	0.018	19.52	0.29	20.27	0.00212
278.15	1.560	0.020	32.37	0.40	32.70	0.000592
283.15	1.561	0.014	51.14	0.52	51.94	0.000919
288.15	1.565	0.012	80.56	0.87	80.92	0.00028
293.15	1.561	0.014	122.0	0.9	124.7	0.00135
298.15	1.557	0.019	187.3	3.5	189.1	0.000608
303.15	1.541	0.017	287.5	2.5	284.6	0.000662
268.15	0.545	0.020	34.60	1.47	34.64	0.0000622
273.15	0.545	0.017	56.95	1.96	56.57	0.000398
278.15	0.549	0.021	93.74	3.69	90.09	0.00245
283.15	0.558	0.015	147.4	4.4	139.8	0.00335
288.15	0.551	0.014	234.7	7.7	219.6	0.00434
293.15	0.556	0.013	366.5	7.2	332.7	0.00653
298.15	0.549	0.013	566.6	9.4	507.2	0.00770

Continued on next page

Table 4.4. Continued from the previous page.

[a]Temperature T [K]	Pressure		Measured		Calculation	
			Mole fraction of Hg		Mole fraction of Hg	[b]ARLD
	P [MPa]	u (P) [MPa]	$y_2 \times 10^9$ [-]	u (y_2) $\times 10^9$ [-]	$y_2 \times 10^9$ [-]	$\lvert\Delta\log_{10} y_2\rvert$ [-]
303.15	0.552	0.014	819.6	23.5	749.4	0.00639

[a]u (T) = 0.05 K

[b]ARLD: absolute relative logarithmic deviation

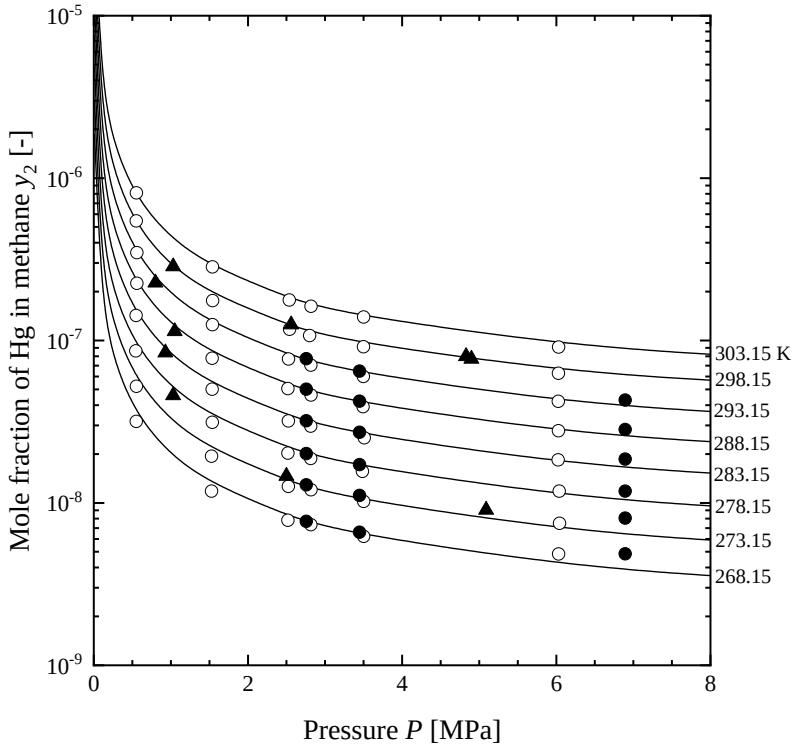

Fig. 4.3. Hg solubility in methane: this work (○); Butala et al. [11] (●); Chapoy et al. [12] (▲); PR/PRSV-EOS (——).

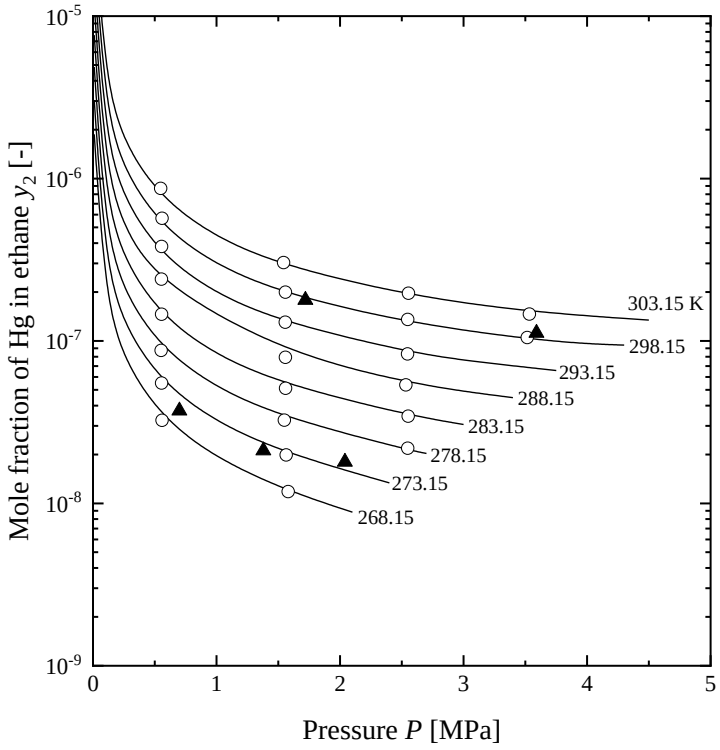

Fig. 4.4. Hg solubility in ethane: this work (○); Chapoy et al. [12] (▲); PR/PRSV-EOS (——).

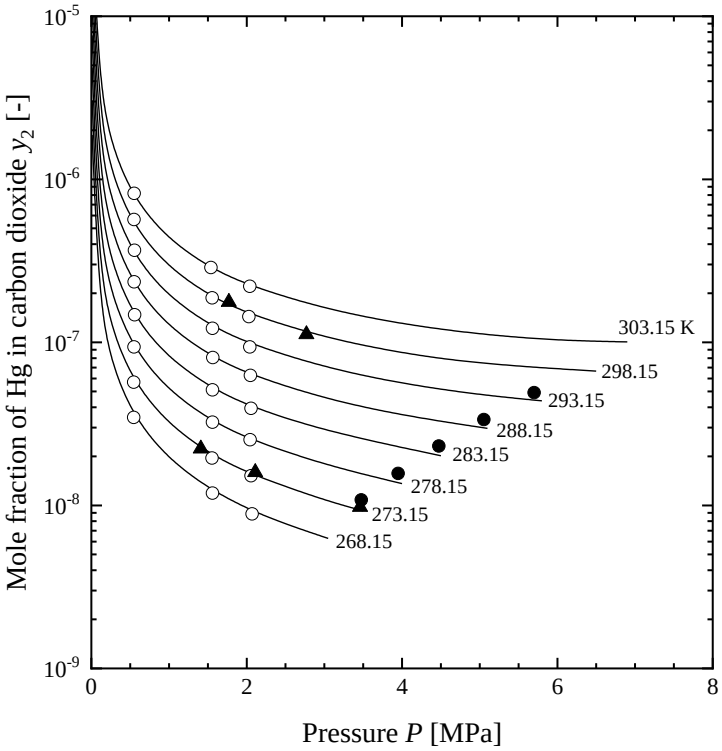

Fig. 4.5. Hg solubility in carbon dioxide: this work (○); Butala et al. [11] (●); Chapoy et al. [12] (▲); PR/PRSV-EOS (——).

Fig. 4.6 shows the van't Hoff plots of saturated the Hg solubility in gaseous methane, ethane, and carbon dioxide using the data around 1.5 MPa and 3.5 MPa. The plots for carbon dioxide are just at 1.558 MPa. The data were correlated with the following equation:

$$\ln y_2 - \ln y_{2,298.15K} = -\frac{\Delta H}{R}\left(\frac{1}{T} - \frac{1}{298.15}\right) \tag{22}$$

where $y_{2,298.15K}$ and ΔH are the Hg solubility at the reference temperature of 298.15 K and the dissolution enthalpy, respectively. The slopes for methane of the two isobars in **Fig. 4.6** were the same. The resulting dissolution enthalpies at 1.537 MPa and 3.489 MPa were 61.01 kJ· mol^{-1} and 59.89 kJ· mol^{-1}, respectively. The van't Hoff plots for the three compounds have similar tendencies at 1.5 MPa, and the dissolution enthalpies were 62.59 kJ· mol^{-1} and 61.28 kJ· mol^{-1} for ethane and carbon dioxide, respectively. These values were close to methane at 1.537 MPa and the vaporization enthalpy of Hg, which was 62.90 kJ· mol^{-1}. The results suggest that the interaction of the molecules between Hg and the pure gases is a little. Although the van't Hoff plots were unavailable for carbon dioxide around 3.5 MPa, those for methane and ethane were slightly different. The dissolution enthalpies of methane at 3.489 MPa and ethane at 3.527 MPa were 59.89 and 50.10 kJ· mol^{-1}, respectively. The results suggest that ethane enhances Hg solubility near the saturated pressure. However, further investigation is required for confirmation.

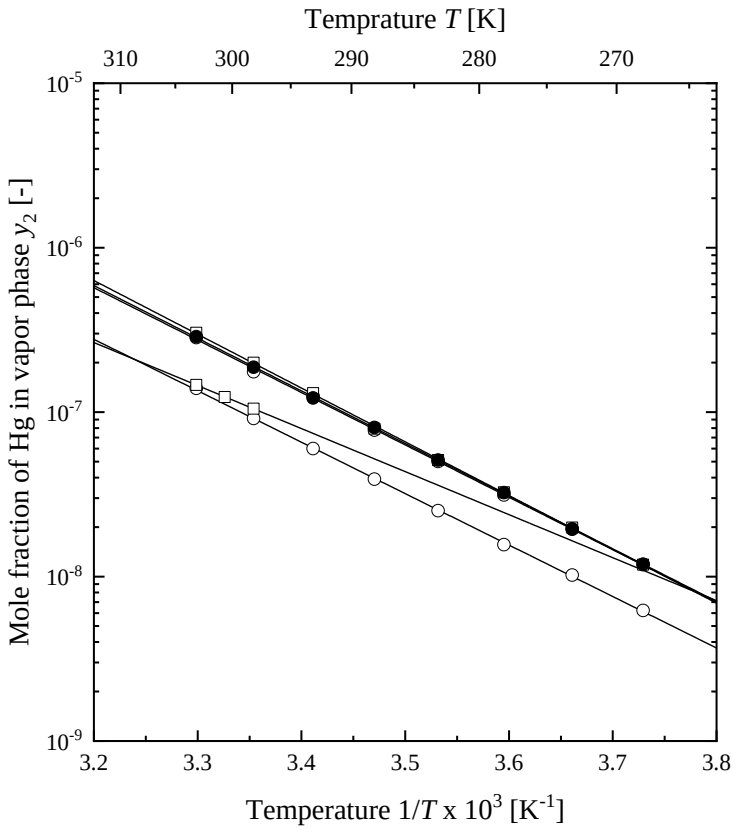

Fig. 4.6. van't Hoff plots of Hg solubility in methane (○) at 1.537±0.007 and 3.489±0.013 MPa; ethane (□) at 1.559±0.022; 3.527±0.011 MPa, and carbon dioxide (●) at 1.558± 0.017 MPa; Eq. (22) (——).

4.1.3 Modeling of vapor-liquid equilibrium of Hg in pure gases

Although there are only a few data points on gas solubilities in liquid Hg, helium solubility has just been reported by Hasegawa et al. [57]. Their reported mole fraction of helium in liquid Hg was 1.53×10^{-6} at 0.362 MPa and 300 K. Considering the gas concentration in liquid Hg, the elemental Hg phase can be assumed to be a liquid without immiscibility or a solid with fluidity. Therefore, as shown in **Eq. (17)**, the fugacity of the Hg phase is equal to that of the elemental Hg. **Eq. (17)** has a similar function to the fugacity of solid [58], and the saturated vapor pressure and the saturated molar volume are evaluated by the PR-EOS. For vapor-liquid equilibrium of Hg in pure gases, components 1 and 2 correspond to the pure gas and elemental Hg, respectively. Therefore, elemental Hg is just in the vapor and liquid phase. The equilibrium condition is given by **Eq. (18)**.

The saturated Hg vapor pressure estimated by the PR-EOS is shown in **Fig. 4.1**. Although

its temperature dependence was similar to those found experimentally, the estimated values differed significantly from the experimental data. The temperature dependence of the attractive parameter was investigated to correlate the PR-EOS to the experimental data. **Fig. 4.7** shows the value of α in the PR-EOS calculated from experimental data. The attractive parameter did not depend on the temperature in the experimental range. As the resistivity of Hg is very low, only coulombic interaction is present among the Hg molecules. Coulombic force does not have temperature dependence. Therefore, the attractive parameter seemed not to have temperature dependence. A similar result for the attractive parameter has been reported for a polymer [59]. By fitting the values of α, a constant value could be determined in the following equation:

$$a = 0.45724 \frac{R^2 T_c^2}{P_c} \times 1.1036 \tag{23}$$

The saturated vapor pressure of Hg calculated by the PR-EOS with **Eq. (23)** is shown in **Fig. 4.1**; the results showed a similar tendency to that of **Eq. (7)**. The PR-EOS calculated the liquid density both with and without **Eq. (23)**. The density of Hg was estimated to be 27.715 and 27.742 g· cm^{-3} at 298.15 K with and without **Eq. (23)**, respectively. This estimate was not sufficient when compared with the actual density of Hg, 13.487 g· cm^{-3} at 298.15 K [47]. However, this error did not occur when using **Eq. (1)**. Therefore, the improvement was just for the saturated vapor pressure. **Eq. (23)** was used to estimate Hg solubility in the vapor and liquid in this research phase.

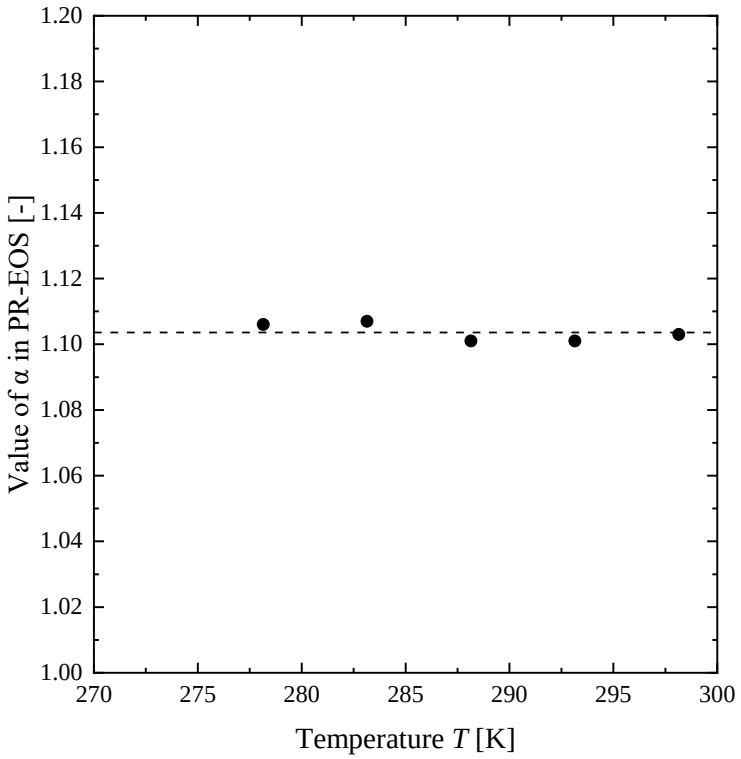

Fig. 4.7. Value of α in the PR-EOS calculated from experimental data: this work (●); α = 1.1036 (·····).

The calculation results of Hg solubility in methane, ethane, and carbon dioxide by the PR/PRSV-EOS are shown in **Figs. 4.3** to **4.5**. When the temperature dependence was implemented for the binary interaction parameter as shown in **Eq. (15)**, the calculations showed a good agreement with the experimental data. The reproducibility was assessed by the absolute relative logarithmic deviation (ARLD):

$$\left|\Delta \log_{10} y_2\right| = \left|\frac{\log_{10} y_2^{\,cal} - \log_{10} y_2^{\,\exp}}{\log_{10} y_2^{\,\exp}}\right| \tag{24}$$

The ARLDs for methane ethane, and carbon dioxide are listed in **Tables 4.2** to **4.4**.

Table 4.5 lists the binary interaction parameters k_{ij} fitted with the Hg mole fraction in the vapor phase, and **Figs. 4.8** to **4.10** shows their temperature dependence. The value of the binary interaction parameter was determined by minimizing with the following objective function (*OF*):

$$OF = \left(f_2^V - f_2^L \right)^2 \tag{25}$$

Table 4.5. Coefficients in binary interaction parameter for PR-EOS

	Coefficients in binary interaction parameter k_{ij}		
	k_{ij}^0 (= k_{ji}^0) [-]	k_{ij}^1 (= k_{ji}^1) [K^{-1}]	k_{ij}^2 (= k_{ji}^2) [K]
methane (1) – mercury (2)	-1.220	0	438.57
ethane (1) – mercury (2)	-36.67	0.065916	6021.87
carbon dioxide (1) – mercury (2)	-1.754	0	610.30

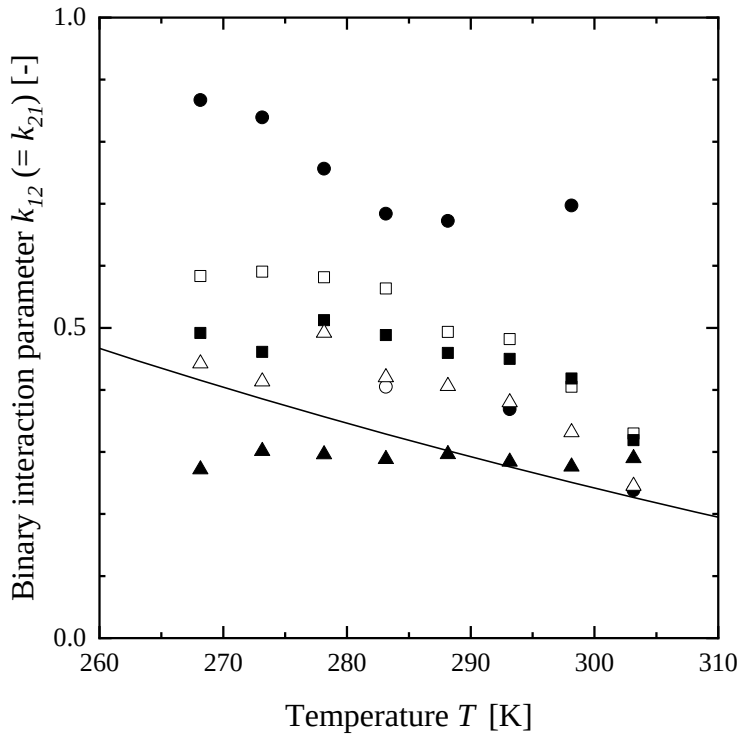

Fig. 4.8. Temperature dependence of binary interaction parameter in PR/PRSV-EOS for methane (1) – Hg (2).; 0.5 MPa, fitted (○); 1.5 MPa, fitted (●); 2.5 MPa, fitted (□); 2.8 MPa, fitted (■); 3.5 MPa, fitted (△); 6.0 MPa, fitted (▲); Eq. (15) (——).

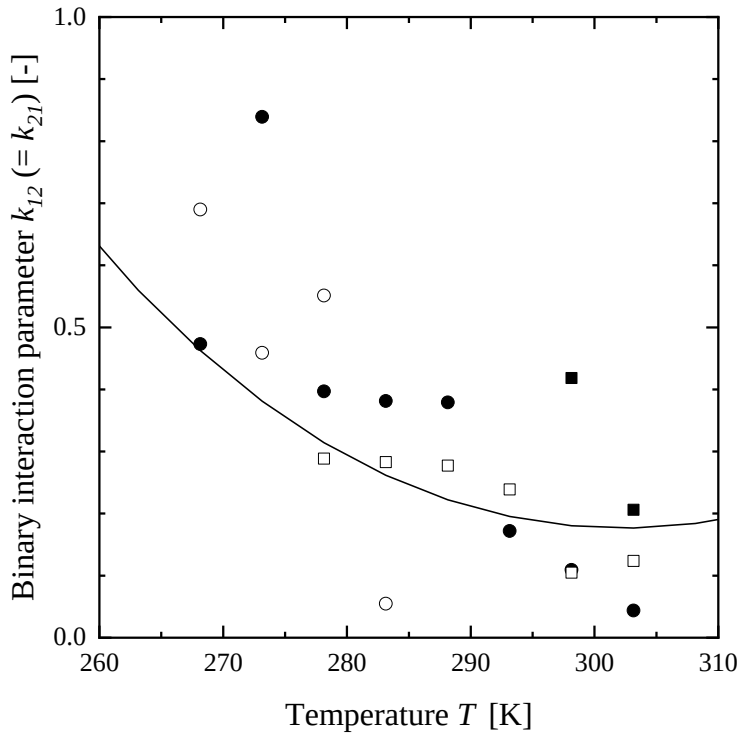

Fig. 4.9. Temperature dependence of binary interaction parameter in PR/ PRSV-EOS for ethane (1) – Hg (2).; 0.5 MPa, fitted (○); 1.5 MPa, fitted (●); 2.5 MPa, fitted (□); 3.5 MPa, fitted (■); Eq. (15) (——).

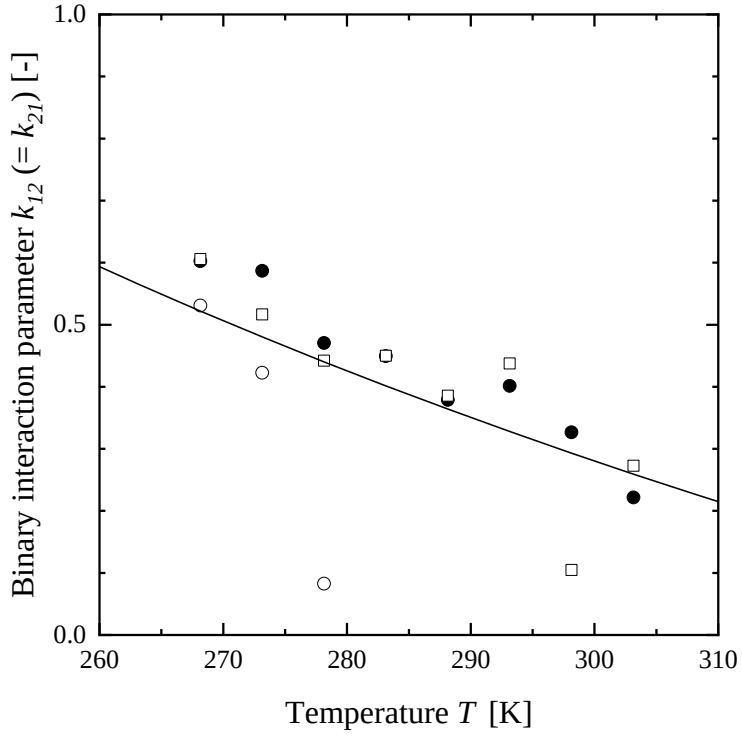

Fig. 4.10. Temperature dependence of binary interaction parameter in PR/PRSV-EOS for carbon dioxide (1) – Hg (2).; 0.5 MPa, fitted (○); 1.5 MPa, fitted (●); 2.0 MPa, fitted (□); Eq. (15) (——).

Figs. 4.11 to 4.13 show the calculation results of the PR-EOS for methane, ethane, and carbon dioxide, respectively, where the pressure is extended to 20 MPa. In the high-pressure region, all calculations were different from the data by Chapoy et al. [12]. The calculation values of the Hg solubility in the liquid phase for ethane and carbon dioxide decreased in the low-temperature region in contrast with that in the high-temperature region. As Chapoy et al. [12] found that the sensitivity of the binary interaction parameter for Hg solubility in the vapor phase was lower than that in the liquid phase, it is considered that this discrepancy was caused by the binary interaction parameters in the PR-EOS, which were determined by the Hg solubility in the vapor phase in this study. Since there was no discrepancy up to around 7 MPa, the standard operating pressure in natural gas processing facilities, there are no practical issues for using of the PR-EOS to calculate Hg partitioning in natural gas processing facilities.

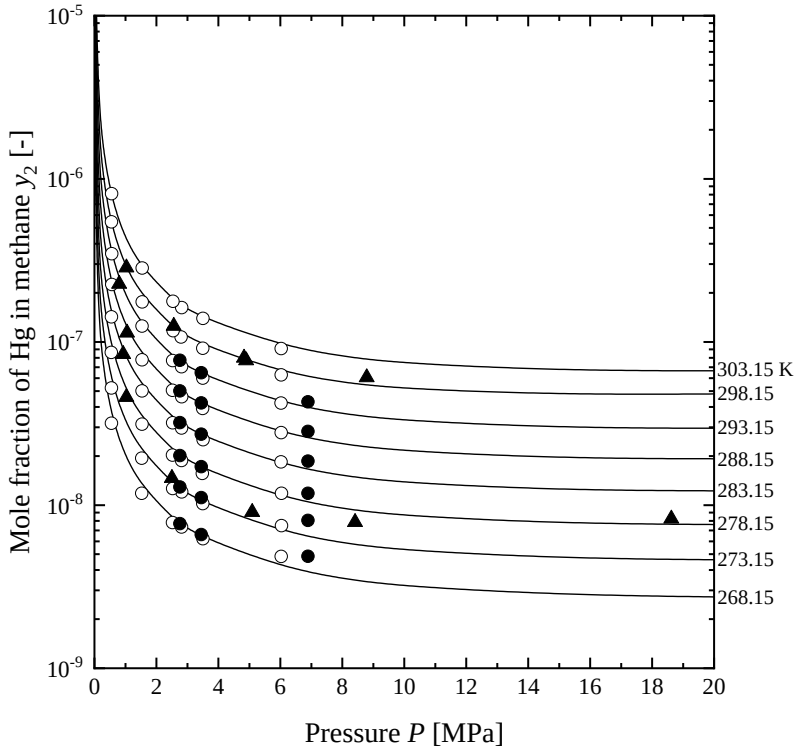

Fig. 4.11. Hg solubility in methane up to 20 MPa: this work (○); Butala et al. [11] (●); Chapoy et al. [12] (▲); PR/PRSV-EOS (——).

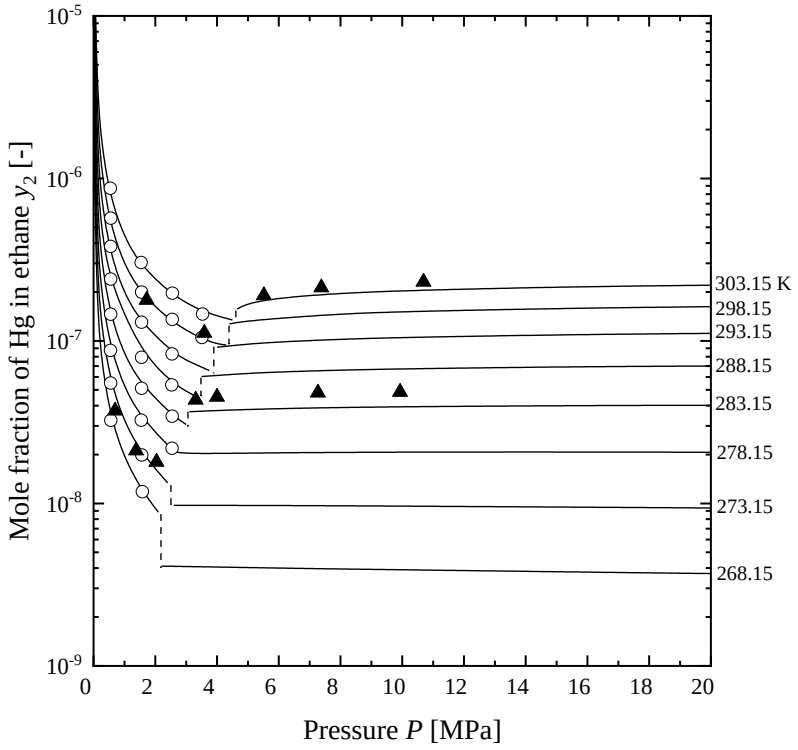

Fig. 4.12. Hg solubility in ethane up to 20 MPa: this work (○); Chapoy et al. [12] (▲); PR/PRSV-EOS (——).

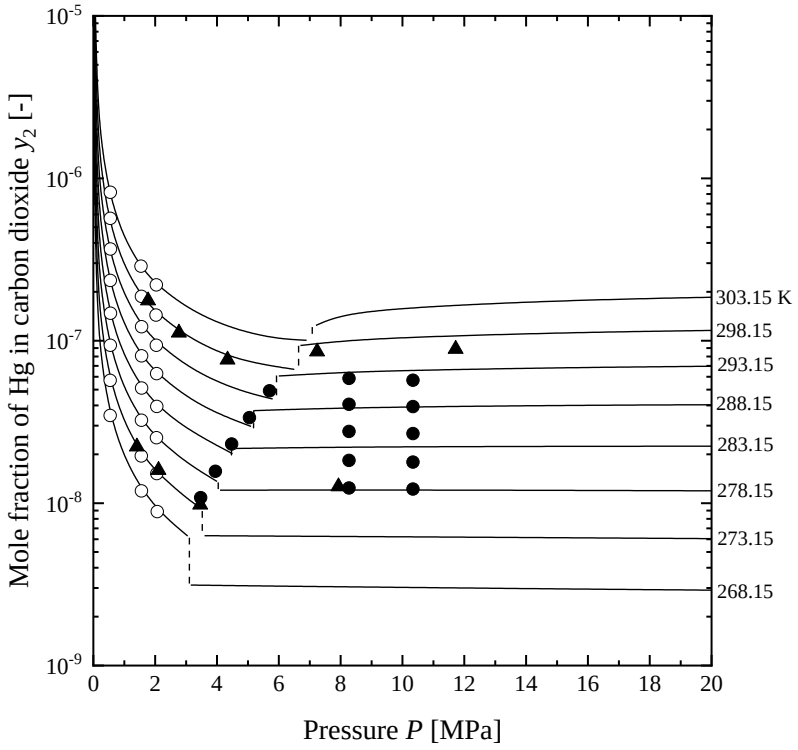

Fig. 4.13. Hg solubility in carbon dioxide up to 20 MPa: this work (○); Butala et al. [11] (●); Chapoy et al. [12] (▲); PR/PRSV-EOS (——).

4.2 Vapor-liquid equilibrium of Hg in artificial natural gas

4.2.1 Measurement of Hg solubility in artificial natural gas

Table 4.6 lists the experimental data of Hg solubility in the artificial natural gas, and **Fig. 4.14** shows its eight isotherms. The isotherm showed a similar pressure dependence to the Hg solubility in methane. The Hg solubility decreased with rising pressure and seemed to be a constant or minimum. The physical properties of elemental Hg seemed similar to organic solids because of its very low miscibility. Although elemental Hg was defined as the liquid phase, its solubility was similar to that of solid organic compounds in SVE.

Table 4.6. Hg solubility in artificial natural gas

[a]Temperature	Pressure		Measured		Calculation	
			Mole fraction of Hg		Mole fraction of Hg	[b]ARLD
T [K]	P [MPa]	u (P) [MPa]	$y_4 \times 10^9$ [-]	u (y_4) $\times 10^9$ [-]	$y_4 \times 10^9$ [-]	$\lvert\Delta\log_{10} y_4\rvert$
268.15	6.031	0.023	4.991	0.049	5.050	0.0618
273.15	6.009	0.034	8.157	0.072	8.123	0.0221
278.15	6.010	0.045	11.92	0.10	11.93	0.00544
283.15	6.002	0.033	18.36	0.10	18.37	0.00262
288.15	6.027	0.030	27.93	0.13	27.90	0.00684
293.15	6.008	0.032	43.02	0.30	42.97	0.00647
298.15	6.009	0.034	63.72	0.43	63.67	0.00521
303.15	6.027	0.031	92.25	0.68	92.20	0.00362
268.15	3.489	0.029	6.481	0.235	6.870	0.310
273.15	3.482	0.034	9.907	0.103	10.10	0.105
278.15	3.487	0.028	16.13	0.23	16.50	0.128
283.15	3.492	0.034	24.66	0.23	25.00	0.0792
288.15	3.503	0.026	39.14	0.36	39.80	0.0975

Continued on next page

Table 4.6. Continued from the previous page.

[a]Temperature T [K]	Pressure		Measurement		Calculation	[b]ARLD
			Mole fraction of Hg		Mole fraction of Hg	
	P [MPa]	u (P) [MPa]	$y_2 \times 10^9$ [-]	u (y_2) $\times 10^9$ [-]	$y_2 \times 10^9$ [-]	$\lvert\Delta\log_{10} y_2\rvert$ [-]
293.15	3.505	0.022	58.92	0.36	59.50	0.0588
298.15	3.495	0.020	91.14	0.90	92.80	0.112
303.15	3.492	0.021	138.7	4.9	142.0	0.147
268.15	2.542	0.029	8.157	0.133	8.420	0.171
273.15	2.508	0.022	13.22	0.17	13.50	0.115
278.15	2.512	0.033	21.08	0.46	21.80	0.190
283.15	2.513	0.034	32.96	0.59	33.90	0.163
288.15	2.506	0.029	51.21	0.68	52.20	0.114
293.15	2.543	0.016	76.95	0.49	77.80	0.0673
298.15	2.540	0.027	121.4	4.7	125.0	0.185
303.15	2.555	0.022	176.6	6.5	181.0	0.160
268.15	1.557	0.025	12.50	0.23	12.90	0.183
273.15	1.538	0.026	21.30	0.52	22.20	0.233
278.15	1.544	0.022	31.84	0.55	32.90	0.189
283.15	1.548	0.024	50.28	0.78	51.70	0.166
288.15	1.552	0.026	78.32	1.30	80.60	0.175
293.15	1.549	0.024	123.0	4.7	127.0	0.202
298.15	1.546	0.026	187.0	7.5	194.0	0.238
303.15	1.556	0.026	278.4	7.7	285.0	0.155
268.15	0.549	0.027	32.44	1.62	35.10	0.457
273.15	0.549	0.022	53.33	2.52	57.70	0.470
278.15	0.551	0.015	86.89	2.81	91.60	0.325

Continued on next page

Table 4.6. Continued from the previous page.

[a]Temperature T [K]	Pressure		Measurement		Calculation	
			Mole fraction of Hg		Mole fraction of Hg	[b]ARLD
	P [MPa]	u (P) [MPa]	$y_2 \times 10^9$ [-]	u (y_2) $\times 10^9$ [-]	$y_2 \times 10^9$ [-]	$\lvert\Delta \log_{10} y_2\rvert$ [-]
283.15	0.550	0.018	142.6	7.2	152.0	0.406
288.15	0.555	0.020	226.5	9.8	244.0	0.488
293.15	0.541	0.021	366.4	19.1	402.0	0.626
298.15	0.548	0.018	551.6	22.8	593.0	0.503
303.15	0.545	0.017	812.5	32.7	879.0	0.561

[a]u (T) = 0.05 K

[b]ARLD: absolute relative logarithmic deviation

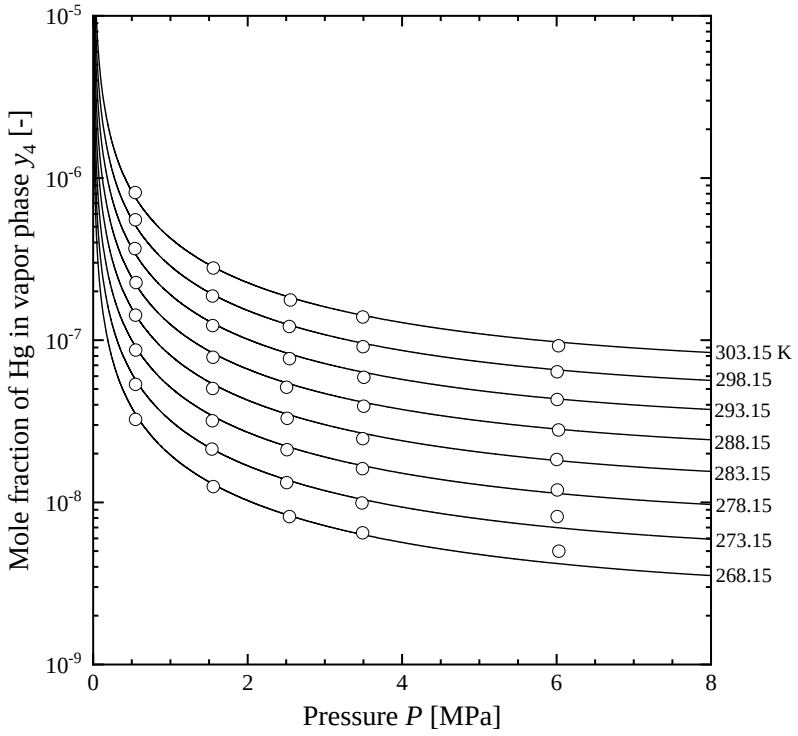

Fig. 4.14. Hg solubility in artificial natural gas: this work (○); PR/PRSV-EOS: (——)

4.2.2 Correlation of vapor-liquid equilibrium of binaries among methane, ethane, and carbon dioxide

Fig. 4.15 shows the literature data of the VLE for methane (1) – ethane (2) reported at 270.00 K [60, 61, 62, 63] and 280.00 K [60]. **Fig. 4.16** shows the literature data of VLE for ethane

(2) – carbon dioxide (3) reported at 270.00 K [63, 64], 283.15 K [65], 288.15 K [65], 291.15 K [65], 293.15 K [65], and 298.15 K [65]. **Fig. 4.17** shows the literature data of VLE for methane (1) –carbon dioxide (3) reported at 270.00 K [63, 66, 67, 68], 271.48 K [69], 273.15 K [70], 288.15 K [70], 288.5 K [71], and 293.4 K [71]. In **Fig. 4.17**, the calculations were shown at 293.4 K, 288.5 K, and 270.00 K. The binary interaction parameters k_{ij} were evaluated for three binaries, methane – ethane, ethane – carbon dioxide, and methane – carbon dioxide. The parameters were determined such that the critical point, or the azeotropic point, was reproduced for the three binaries. As shown in **Fig. 4.18 to 4.20**, the parameters were given as a linear function of temperature. **Table 4.7** lists the coefficients for **Eq. (15)**.

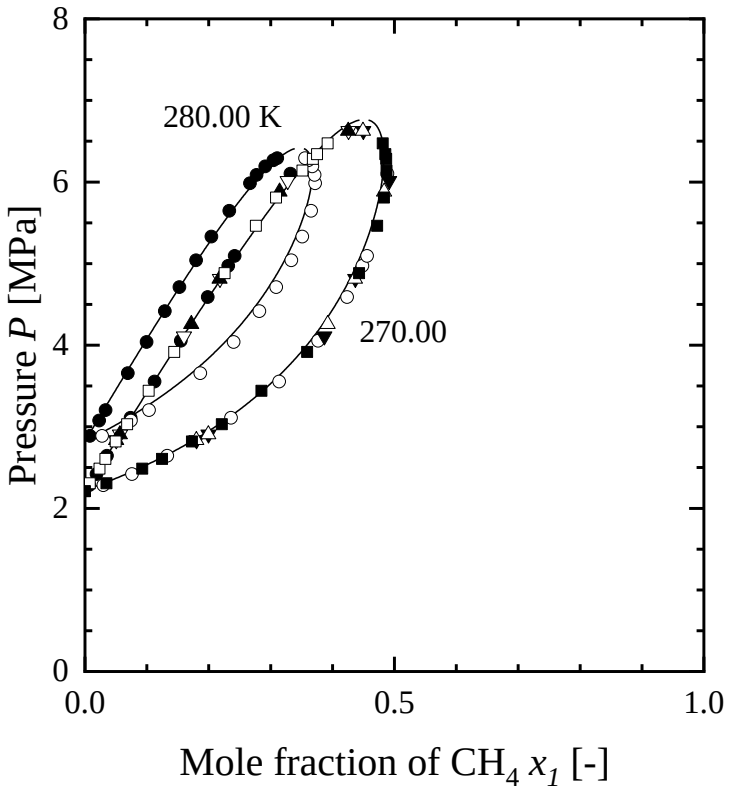

Fig. 4.15. Vapor-liquid equilibrium for methane (1) – ethane (2): Gupta et al. at 270.00 K and 280.00 K [60] (○, ●); Raabe et al. at 270.00 K [61] (□, ■); Janisch et al. at 270.00K [62] (△, ▲); Wei et al. at 270.00 K [63] (▽, ▼); PR/PRSV-EOS: (——).

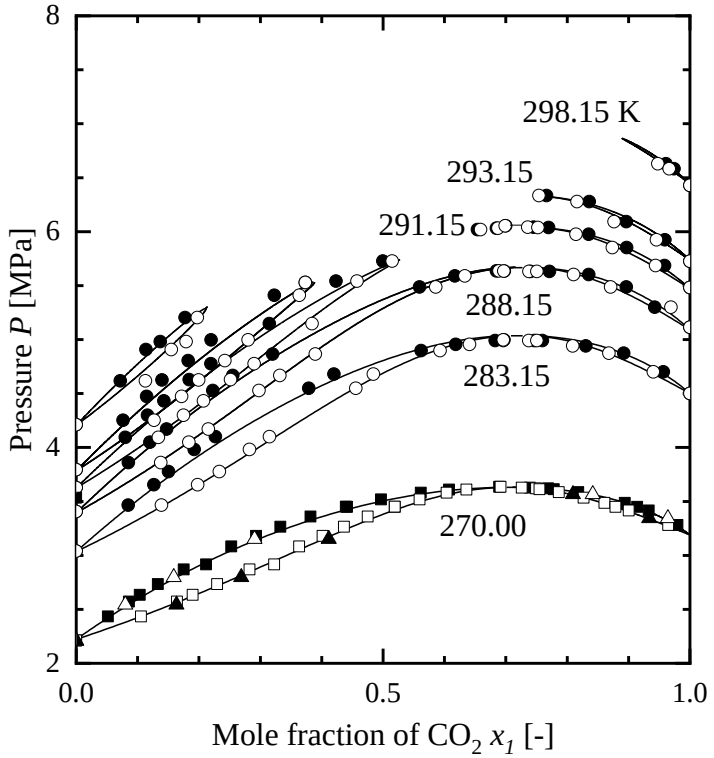

Fig. 4.16. Vapor-liquid equilibrium for ethane (2) – carbon dioxide (3): Wei et al. at 270.00 K [63] (△, ▲); Brown et al. at 270.00 K [64] (□, ■); Ogaki and Katayama at 283.15 K, 288.15 K, 291.15 K, 293.15 K, and 298.15 K [65] (○, ●); PR/PRSV-EOS: (——).

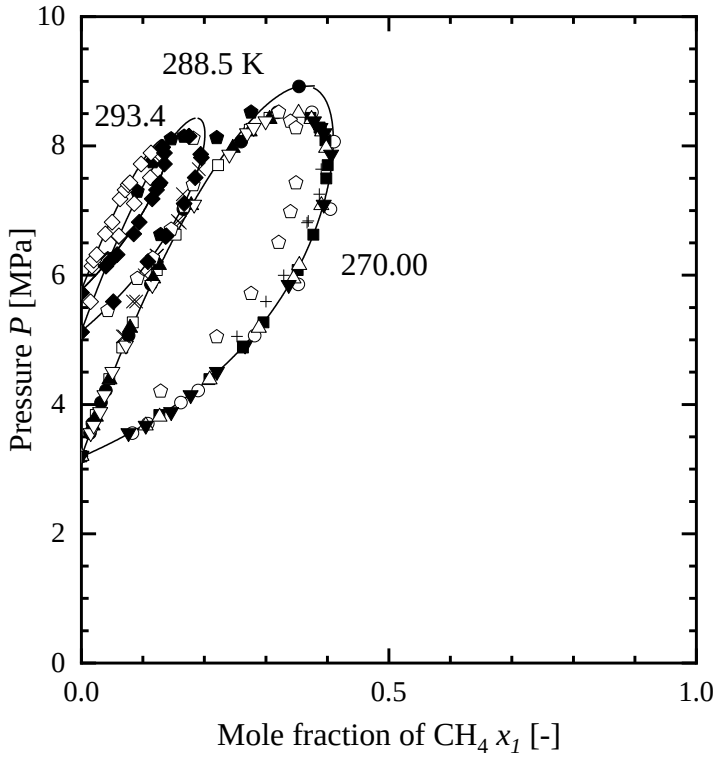

Fig. 4.17. Vapor-liquid equilibrium for methane (1) – carbon dioxide (3): Davalos at 270.00 K [66] (○, ●); Somait and Kidnay at 270.00 K [67] (□, ■); Al-Sahhaf et al. at 270.00 K [68] (△, ▲); Wei et al. at 270.00 K [65] (▽, ▼); Donnelly and Katz at 271.48 K [69] (×, +); Arai et al. at 273.15 K and 288.15 K [70] (⬠, ⬟); Xu et al. at 288.5 K and 293.4 K [71] (◇, ◆); PR/PRSV-EOS: (——).

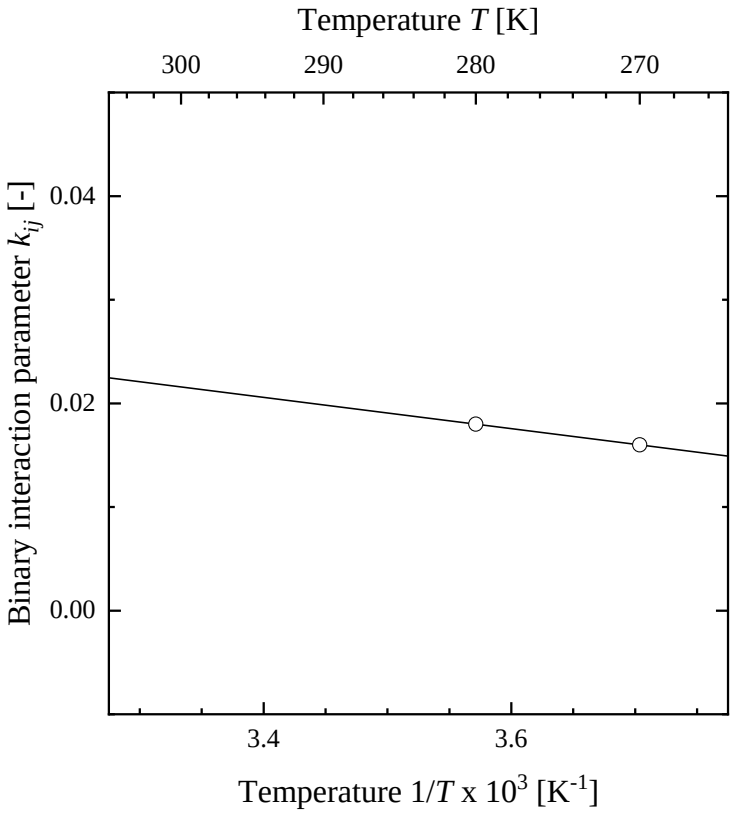

Fig. 4.18. Temperature dependence of binary interaction parameter in PR/PRSV-EOS for methane (1) – ethane (2).

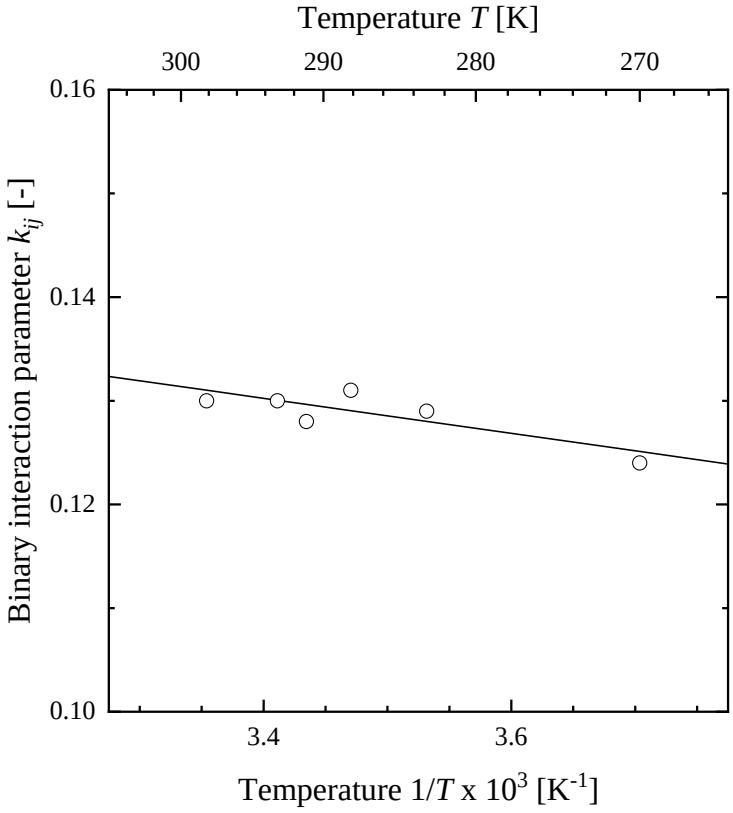

Fig. 4.19. Temperature dependence of binary interaction parameter in PR/PRSV-EOS for ethane (2) – carbon dioxide (3).

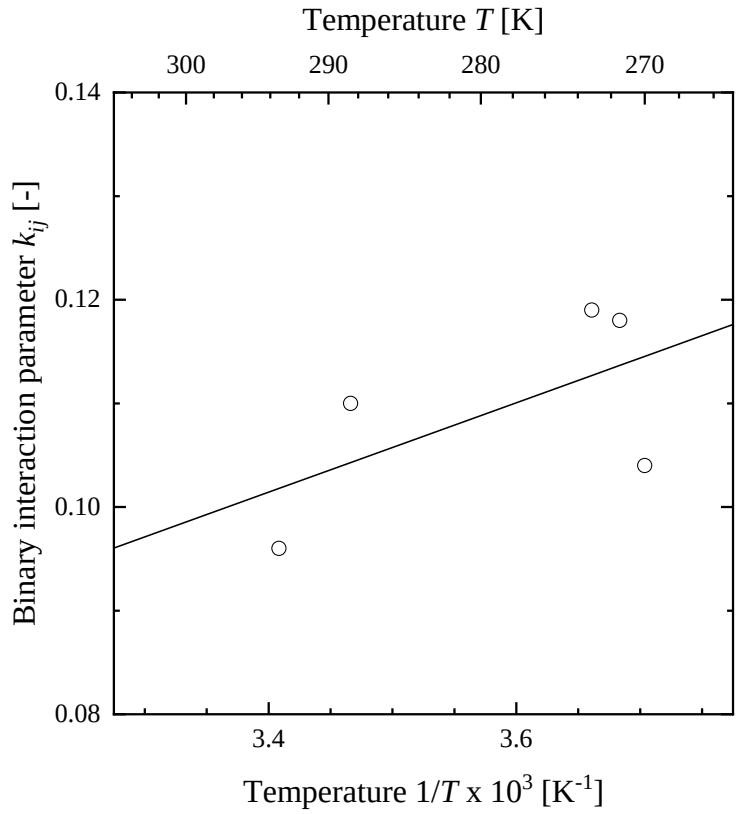

Fig. 4.20. Temperature dependence of binary interaction parameter in PR/PRSV-EOS for methane (1) – carbon dioxide (3).

Table 4.7. Coefficients in binary interaction parameter for PR/PRSV-EOS

	Coefficients in binary interaction parameter k_{ij}		
	k_{ij}^0 (= k_{ji}^0) [-]	k_{ij}^1 (= k_{ji}^1) [K^{-1}]	k_{ij}^2 (= k_{ji}^2) [K]
methane (1) – ethane (2)	0.07199	-0.01512	0.00
methane (1) – carbon dioxide (3)	-0.04528	0.04315	0.00
[a]methane (1) – mercury (4)	-1.220	0.00000	438.57
ethane (2) – carbon dioxide (3)	0.1877	-0.01690	0.00
[a]ethane (2) – mercury (4)	-39.68	0.06592	6021.87
[a]carbon dioxide (3) – mercury (4)	-1.754	0.00000	610.30

[a]from Table 4.5

4.2.3 Modeling Hg solubility in artificial natural gas

Table 4.7 lists the coefficients in **Eq. (15)** for methane - Hg, ethane – Hg, and carbon dioxide – Hg. These were determined in section **4.1.3.** The Hg solubility was calculated using the six binary interaction parameters for the artificial natural gas. **Table 4.6 and Fig. 4.14** show the

calculation results. The calculation showed good reproducibility with the experimental data. Therefore, the proposed method will be applicable even for the natural gas in the actual conditions. The reproducibility was assessed by the absolute relative logarithmic deviation (ARLD):

$$\left|\Delta \log_{10} y_4\right| = \left|\frac{\log_{10} y_4^{\,cal} - \log_{10} y_4^{\,\exp}}{\log_{10} y_4^{\,\exp}}\right| \tag{26}$$

Chapter 5 Liquid-Liquid Equilibrium of Hg in solvents for natural gas processing

5.1 Measurement of Hg solubility in solvents for natural gas processing

5.1.1 Hg solubility in methanol

Table 5.1 lists the experimental data for the Hg solubility in methanol. The listed u (x_2) values were estimated from the volume ratio for the dilution solvent at the CVAAS, and **Fig. 5.1** shows the temperature dependence of the experimental data. The measurements were performed under a nitrogen atmosphere to avoid the oxidation of elemental Hg. The measurements were also performed in the open air without any nitrogen purge to confirm the effectiveness of the experimental procedures. The data are shown together with those from the literature, Spencer and Voigt [41], Gallup et al. [25], and Corns et al. [27]. All the experimental data correlated well with the equation followed the van't Hoff equation:

$$\ln x_2 - \ln x_{2,298.2K} = -\frac{\Delta H}{R}\left(\frac{1}{T} - \frac{1}{298.2}\right) \tag{27}$$

where $x_{2,298.2K}$ and ΔH are the Hg solubility at a reference temperature, 298.2 K, and the dissolution enthalpy. The $x_{2,298.2K}$ for MEG, DEG, TEG, and MDEA were obtained from the correlation of the experimental data. That for methanol was obtained directly from the experiment. **Table 5.2** lists the values for the experimental data. As shown in **Fig. 5.1**, the experimental data were lower than those of Spencer and Voigt [42], Gallup et al. [26], and Corns et al. [28]. Otherwise, the data without nitrogen purging agreed well with those from the literature. The data of Gallup et al. [26] at 283 and 273 K, and the data of Corns et al. [28] at 289 and 278 K had a similar tendency to an extrapolation of the experimental data. The enhancement of the Hg solubility was likely caused by the oxidation of elemental Hg, considering the low reaction rate in the low-temperature range. Spencer and Voigt [42], Gallup et al. [26], and Corns et al. [28] conducted their experiments with reducing agents, such as tin (II) chloride, to prevent the oxidation of mercury without purging nitrogen. Compared with the data without nitrogen purging, it seems that the reducing agents could not prevent the oxidation of

Hg. The dissolution enthalpy was $\Delta H = 32.13$ kJ· mol^{-1}, and the value was lower than the vaporization enthalpy of Hg, which was 62.90 kJ· mol^{-1}. The result suggests that the interaction between Hg and methanol is strong.

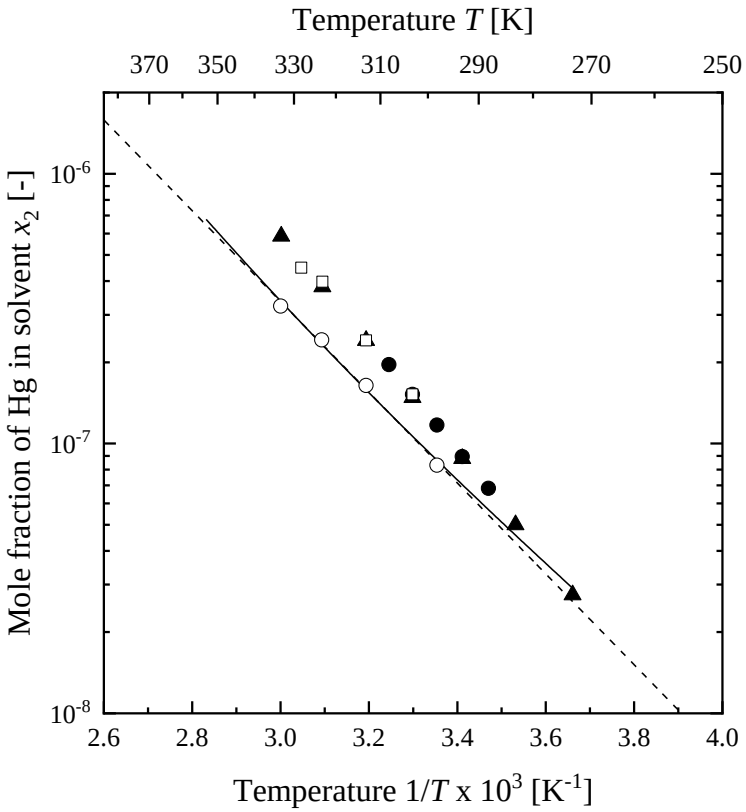

Fig. 5.1. Hg solubility in methanol: this work (○); this work without glove box (□); Spencer and Voigt [42] (●); Gallup et al. [26] (▲); Corns et al. [28] (■); PR/PRSV-EOS: (——); Eq. (27): (- - -).

Table 5.1. Hg solubility in methanol, MEG, DEG, TEG, and MDEA

[a]Temperature T [K]	Measured		Calculated by using Eq. (15)		
	Mole fraction of Hg in liquid phase		Mole fraction of Hg in liquid phase	[b]ARLD	Binary interaction parameter
	$x_2 \times 10^9$ [-]	$u\,(x_2) \times 10^9$ [-]	$x_2 \times 10^9$ [-]	$\lvert\Delta\log_{10}x_2\rvert$ [%]	$k_{12}\,(=k_{21})$ [-]
			Methanol		
298.2	83.1	5.4	86.8	0.264	0.4598
313.2	164	13	158	0.229	0.4864
323.3	242	13	233	0.255	0.5043
333.3	323	15	337	0.278	0.5221
			average	0.256	
			MEG		
303.3	56.5	4.8	58.9	0.247	0.5291
313.3	80.4	6.0	77.9	0.196	0.5558
323.4	108	8	102	0.330	0.5828
333.2	127	6	133	0.276	0.6089
			average	0.262	
			DEG		
303.2	159	10	175	0.611	0.4084
313.2	267	33	235	0.853	0.4377
323.4	314	25	309	0.110	0.4676
333.2	382	28	402	0.339	0.4963
			average	0.478	

Continued on next page

Table 5.1 Continued from previous page

[a]Temperature T [K]	Measured		Calculated by using Eq. (15)		
	Mole fraction of Hg in liquid phase		Mole fraction of Hg in liquid phase	[b]ARLD	Binary interaction parameter
	$x_2 \times 10^9$ [-]	$u\,(x_2) \times 10^9$ [-]	$x_2 \times 10^9$ [-]	$\lvert\Delta \log_{10} x_2\rvert$ [%]	$k_{12}\,(= k_{21})$ [-]
			TEG		
303.2	274	23	279	0.150	0.3433
313.2	380	48	377	0.032	0.3727
323.4	523	32	499	0.337	0.4026
333.4	634	54	655	0.229	0.4320
			average	0.187	
			MDEA		
303.2	180	14	183	0.122	0.4103
313.2	239	22	234	0.138	0.4425
323.4	303	15	295	0.179	0.4753
333.2	361	16	369	0.144	0.5068
			average	0.146	

[a]$u\,(T) = 0.6$ [K]

[b]ARLD: absolute relative logarithmic deviation

Table 5.2. Mole fraction of Hg reference at 298.2 K and apparent enthalpy for Eq. (27)

	Number of Data N	Temperature T [K]		Parameters in Eq. (27)			Ref.
		(lowest)	(highest)	Mole fraction of Hg reference at 298.2 K $x_{2,298.2\ K} \times 10^9$ [-]	Dissolution enthalpy ΔH [kJ· mol^{-1}]	u (ΔH) [kJ· mol^{-1}]	
Methanol	4	298.2	333.3	83.1	32.13	0.11	This work
MEG	4	303.3	333.2	49.8	23.08	0.10	This work
DEG	4	303.2	333.2	149	23.46	0.14	This work
TEG	4	303.2	333.4	238	23.82	0.11	This work
MDEA	4	303.2	333.2	160	19.66	0.13	This work
Pentane	36	258	336	673	43.09	-	10, 19, [a]39, [a]70
Hexane	40	273	338	827	41.56	-	13, 15, 19, 23, [a]39, [a]70
Heptane	12	273	313	952	42.06	-	15, 19
Octane	35	273	336	1086	40.59	-	15, 19, 23, [a]39, [a]70
Decane	11	273.15	336.15	1352	41.33	-	[a]70

[a]Correlation data

5.1.2 Hg solubility in glycols, MEG, DEG, and TEG

Table 5.1 lists the experimental data for the Hg solubility in the three glycols, MEG, DEG, and TEG. **Table 5.2** summarizes the Hg solubility at a reference temperature, 298.2 K, and the dissolution enthalpy for the three glycols. **Figure 5.2** shows the experimental data of the Hg solubility in MEG, together with those of Gallup et al. [26], Li et al. [30], and Corns et al. [28]. The data from Li et al. [30] agreed well with those of Gallup et al. [26] and Corns et al. [28], and the experimental data were lower than those of the three literature reports. However, the data at the lowest temperature reported by Li et al. [30] is quite suspicious because the temperature was below the melting point of MEG, which is T_f = 260.15 K [48]. Therefore, MEG was thought to be in the solid phase or at least a supercool liquid phase. Compared with the data by Gallup et al. [26] and Corns et al. [28], this discrepancy was attributed to the same reason as that in methanol, the oxidation of elemental Hg. **Figure 5.3** shows the Hg solubility in MEG, DEG, and TEG. The data of Gallup et al. [26] and Corns et al. [28] for TEG are also shown. Similar to the data of methanol and MEG, those of Gallup et al. [26] at 293.2 K were slightly larger than the extrapolating value from the experimental data, and the data of Corns et al. [28] at 289 and 278 K had a similar tendency to the extrapolation of the experimental data. Among the three glycols, the dissolution enthalpies were approximately ΔH = 23.45±0.37 kJ· mol^{-1}.

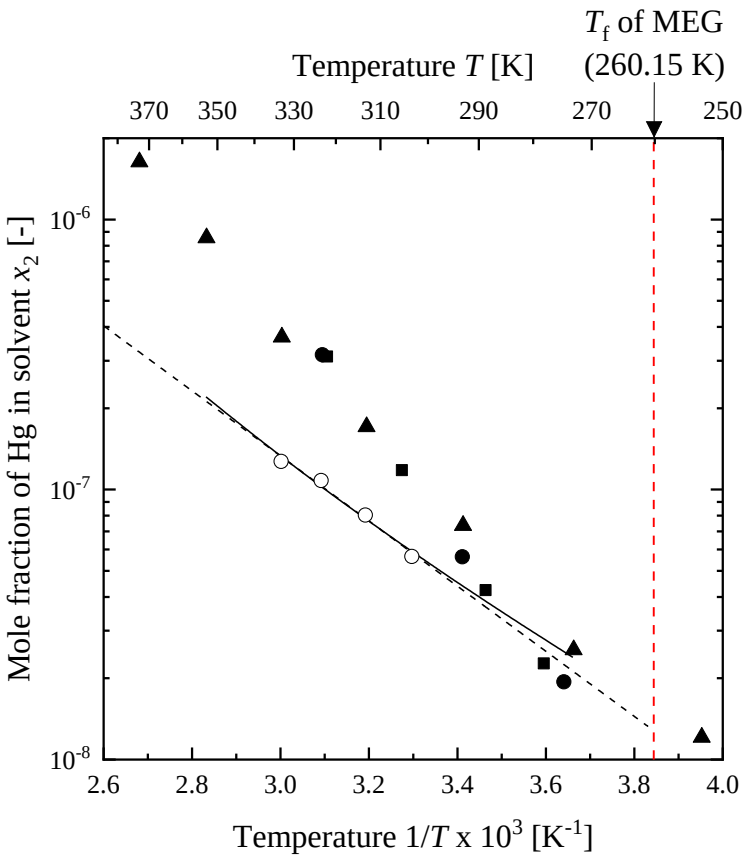

Fig. 5.2. Hg solubility in MEG: this work (○); Gallup et al. [25] (●); Corns et al. [28] (■); Li et al. [30] (▲); PR-EOS: (——); Eq. (27): (- - -); T_f of MEG (- - -).

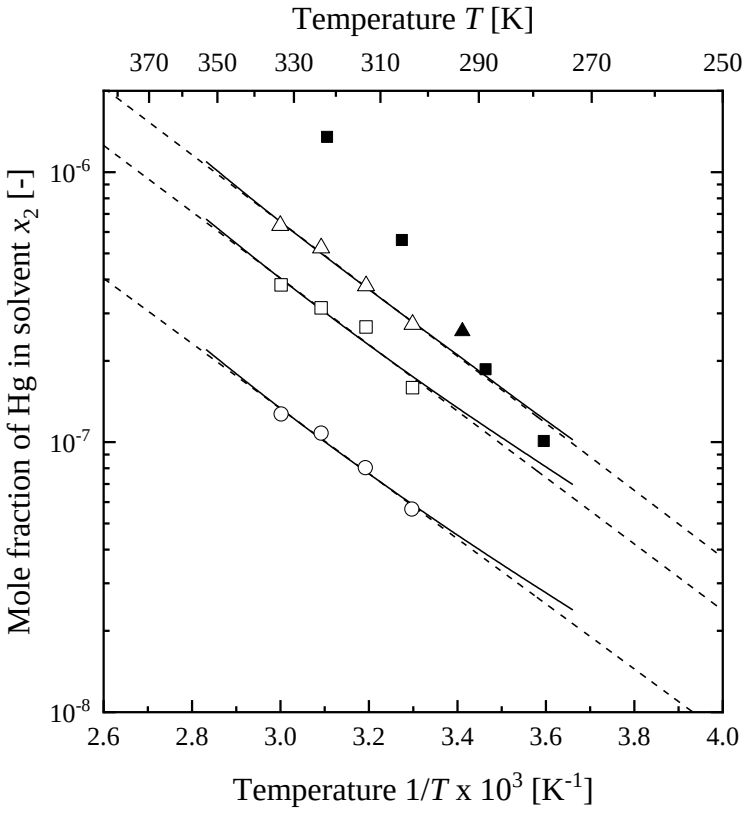

Fig. 5.3. Hg solubility in glycols: this work: MEG: (○); DEG: (□); TEG: (△); Gallup et al. [26]: TEG: (▲); Corns et al. [28]: TEG: (■); PR-EOS: (——); Eq. (27): (- - -).

5.1.3 Hg solubility in MDEA

Table 5.1 lists the experimental Hg solubility data in MDEA, and **Table 5.2** summarizes the Hg solubility at a reference temperature, 298.2 K, and the dissolution enthalpy. **Figure 5.4** shows the experimental data of the Hg solubility in MDEA. The dissolution enthalpy was ΔH = 19.66 kJ·mol^{-1}, and the value was slightly lower than the glycols. However, the Hg mole fraction was a similar value to that in DEG in the experimental temperature range. The molecular structure and the reactivity of MDEA differed from those of DEG. Otherwise, the number of constituent atoms in MDEA, except hydroxyl and methyl groups, was the same as DEG. We consider the relationship between the number of constituent atoms in the solvent molecule and the Hg solubility.

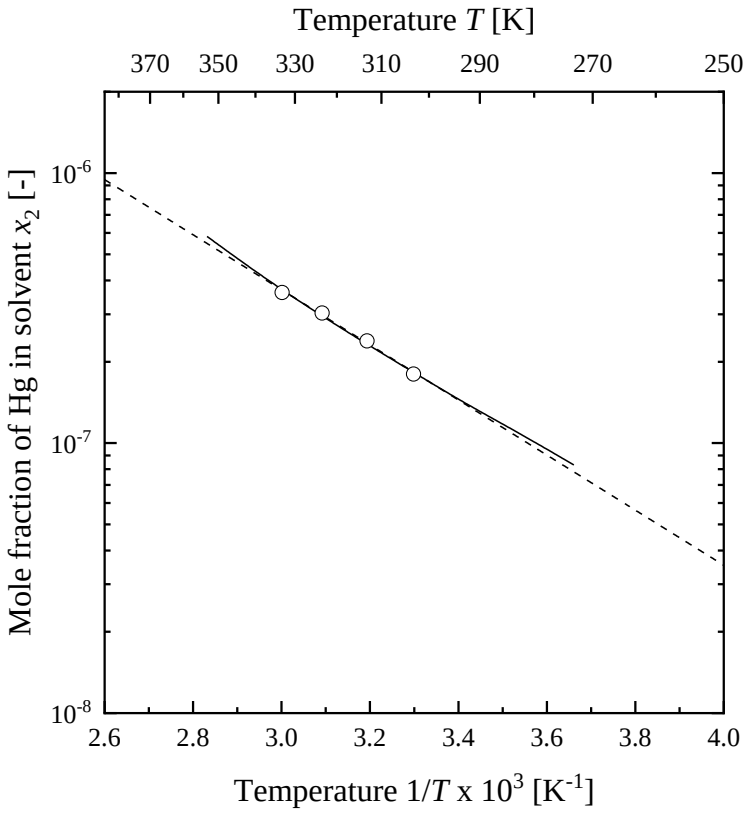

Fig. 5.4. Hg solubility in MDEA: this work (○); PR-EOS (——); Eq. (27): (- - -).

5.2 Reduced Hg solubility for reference solvent

Considering the similarity of Hg solubility in DEG and MDEA, a reduced Hg solubility is

proposed in this study:

$$x_{2r} = \frac{x_2}{x_{2,ref}} \tag{28}$$

where $x_{2,ref}$ is the Hg solubility in the reference solvent at a given temperature. In this study, DEG was used as a reference solvent. **Table 5.3** lists the reduced Hg solubilities for MEG, TEG, and MDEA at the four isotherms, 303.2 to 333.2 K, and **Fig 5.5** shows the comparison of the reduced Hg solubilities. The reduced Hg solubilities were calculated from **Eq. (28)** with the Hg solubility at a reference temperature, 298.2 K and the dissolution enthalpies listed in **Table 5.2**. The dissolution enthalpies for MEG, DEG, and TEG were similar. Furthermore, the Hg solubility in MDEA was almost the same as that in DEG. The number of constituent atoms of MDEA, excluding hydroxyl and methyl groups and hydrogen atoms, is n_A = 5, which is the same as that of DEG. Examples for counting the number of constituent atoms are shown in **Fig. 5.6**. The numbers of constituent atoms are n_A = 2 and 8 for MEG and TEG, respectively. The ratio of the numbers of constituent atoms in MEG : TEG : MDEA was thus 0.40 : 1.60 : 1.00. As shown in **Table 5.3**, this ratio was similar to the reduced Hg solubility, i.e., 0.33 : 1.62 : 0.98. Based on literature data [11, 14, 16, 21, 25] and correlation data [41, 72], the method was applied to consider Hg solubilities in liquid C5 to C8, and C10 aliphatic hydrocarbons at 258 to 338 K. **Figure 5.7** shows the temperature dependences. As shown in **Fig. 5.7**, all data correlated with **Eq. (27)**. **Table 5.2** lists the Hg solubility at a reference temperature, 298.2 K, and the dissolution enthalpy for C5 to C8, and C10 hydrocarbons. The dissolution enthalpies were approximately ΔH = 41.73±1.36 kJ· mol^{-1} for the five hydrocarbons. Although the value of the dissolution enthalpy was larger than those of the three glycols, similar dissolution enthalpies were obtained among the C5 to C8, and C10 aliphatic hydrocarbons. Pentane was used as a reference solvent for the hydrocarbons because the constituent number of atoms is the same as DEG, n_A = 5. **Table 5.3** lists the reduced Hg solubilities for hexane, heptane, octane, and decane for the seven isotherms, 273 to 333 K. The average ratios of the reduced Hg solubilities were 1.22 : 1.41 : 1.60 : 1.99 for the ratio of hexane : heptane : octane : decane. These values were close

to the ratio of the numbers of constituent atoms for hexane, heptane octane, and decane, i.e., 1.20 : 1.40 : 1.60 : 2.00. As the same relationship was observed in both diols and aliphatic hydrocarbons, the mechanism of dissolving elemental Hg in these solvents is presumed physical rather than chemical interaction. **Figure 5.8** depicts the images of dissolving elemental Hg in glycols. Since elemental Hg was presumed to be trapped on a carbon, oxygen or nitrogen atom with the probability about 3×10^{-8} to 6×10^{-8} considering the mole fraction measured in this research, Hg solubility increased with the number of constituent atoms of solvents. Although the theoretical basis for this relationship remains unclear, this method is applicable for solvents with a similar dissolution enthalpy in terms of Hg solubility.

Table 5.3. Reduced Hg solubility x_{2r} and its reference solvent

Temperature T [K]	Reduced Hg solubility x_{2r} [-]						
	$x_{2,ref}$: DEG			$x_{2,ref}$: Pentane			
	MEG	TEG	MDEA	Hexane	Heptane	Octane	Decane
273.2				1.30	1.47	1.77	2.14
283.2				1.27	1.45	1.70	2.09
293.2				1.24	1.43	1.64	2.03
303.2	0.36	1.72	1.13	1.22	1.41	1.59	1.99
313.2	0.30	1.42	0.90	1.19	1.39	1.54	1.94
323.2	0.34	1.67	0.96	1.17	1.37	1.49	1.90
333.2	0.33	1.66	0.95	1.15	1.36	1.45	1.87
average	0.33	1.62	0.98	1.22	1.41	1.60	1.99

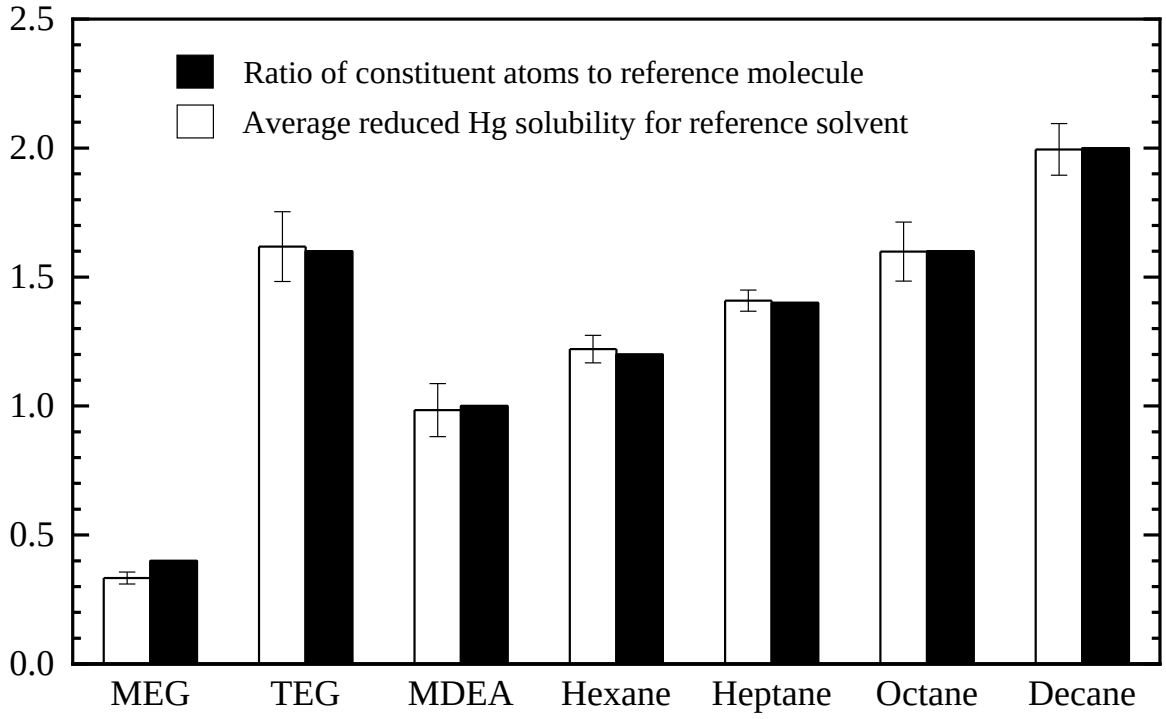

Fig. 5.5. Comparison of ratio of constituent atoms to reference molecule, and reduced Hg solubility x_{2r} listed in Table 5.3.

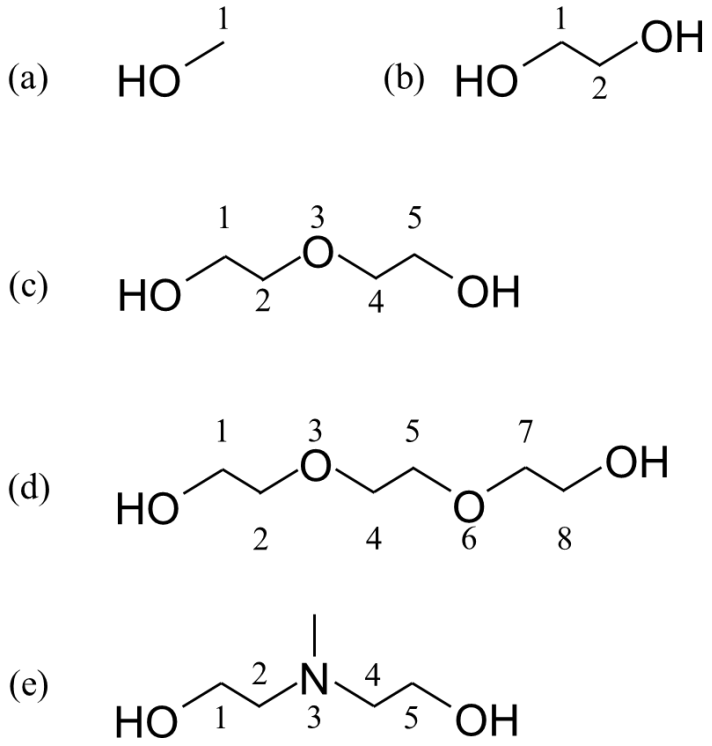

Fig. 5.6. Molecular structure of solvents; (a) methanol; (b) MEG; (c) DEG; (d) TEG; (e) MDEA; Methods for counting n_A are shown beside the molecular formulae.

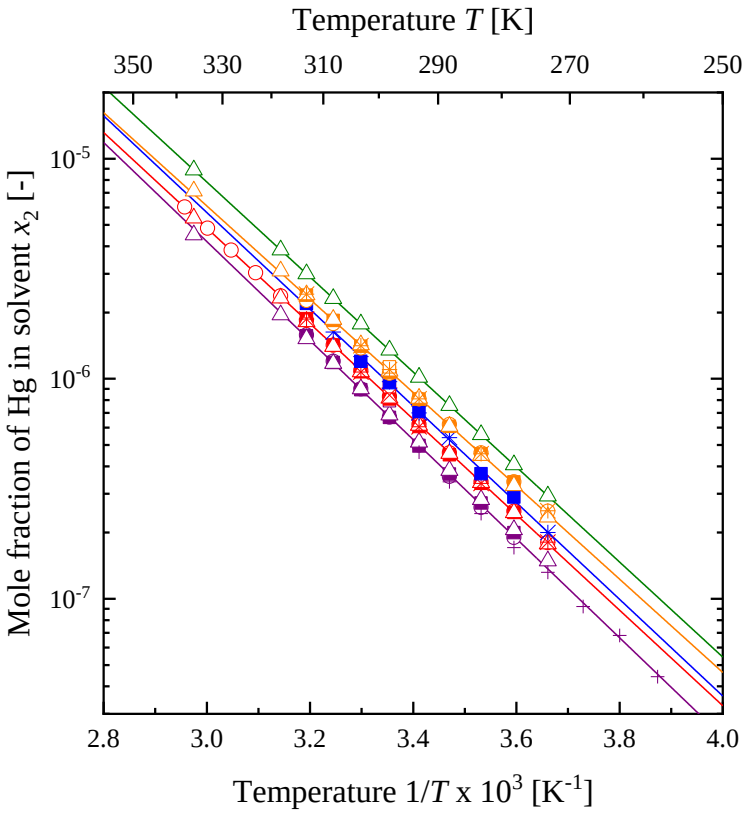

Fig. 5.7. Hg solubility in liquid C5 to C8, and C10 aliphatic hydrocarbons: purple: pentane; red: hexane; blue: heptane; orange: octane; green: decane; Clever [41]: (○); Okouchi and Sasaki [21]: (■); Clever and Iwamoto [72]: (△); Bloom and Gallup [25]: (□); Butala et al. [11]: (+); Kuntz and Mains [14]: (×); Spencer and Voigt [16]: (*); Eq. (27): (———).

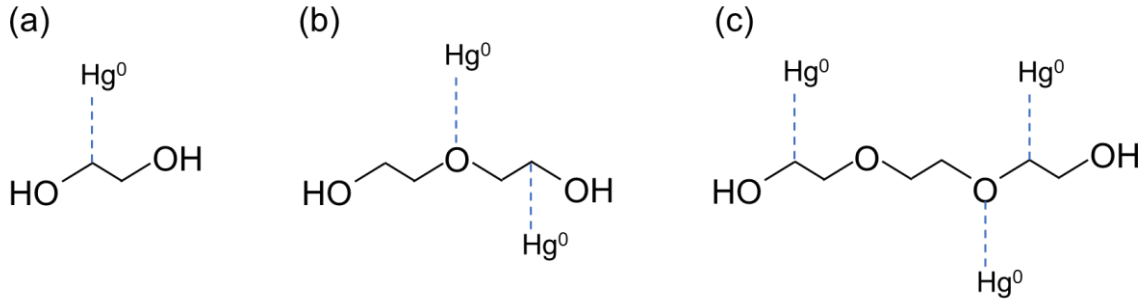

Fig. 5.8. Images of dissolving elemental Hg in glycols: (a) MEG; (b) DEG; (c) TEG.

5.3 Data correlation and prediction of equilibrium pressure and mole fraction of Hg in the vapor phase

The binary system investigated in this study contained three coexisting phases, namely an elemental Hg phase, organic liquid phase, and vapor phase. Thus, the degrees of freedom are $F = 1$ in Gibbs's theorem. Therefore, the equilibrium pressure and the Hg concentration in the vapor phase

should only be evaluated from the Hg mole fraction in the organic liquid phase. **Figure 5.9** shows an example of the phase equilibrium calculation for methanol (1) – Hg (2) at 298.2 K. The calculation is explained as follows:

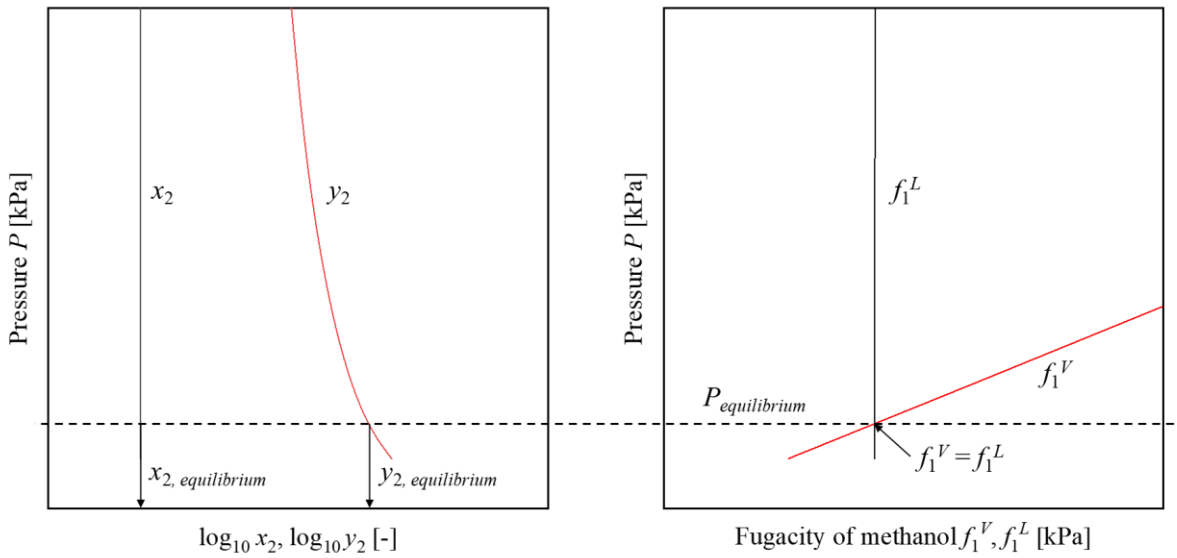

Fig. 5.9. Calculation scheme for three phase equilibrium for methanol (1) - Hg (2) at 298.2 K.

The binary interaction parameter, k_{ij}, was first given by **Eq. (15)**. Successively, **Eqs. (16)** and **(19)** were applied under the assumption that the Hg phase was immiscible with the solvent. As shown in **Fig. 5.9**, pressure dependencies on the Hg mole fractions could be evaluated in the organic liquid and the vapor phases. Then, pressure dependences on the fugacity of methanol were also evaluated at given pressures. The point of intersection, shown in **Fig. 5.9**, was satisfied under the conditions of **Eq. (16)**; hence, the equilibrium pressure, P, could be determined. Considering the self-consistency of **Eq. (15)**, the binary interaction parameter k_{ij} was determined. The value of the binary interaction parameter was determined by minimizing with the following objective function (OF):

$$OF = \left(f_2^L - f_2^{L2} \right)^2 \tag{29}$$

Table 5.4 lists the binary interaction parameters k_{ij} fitted with the Hg mole fraction in the organic liquid phase, and **Fig. 5.10** shows their temperature dependence. Based on **Eq. (15)**, the calculation results are listed in **Table 5.1**, and the Hg solubilities in the organic liquid phase are shown in **Figs.**

5.1 to 5.3. The calculation results of the Hg solubility agreed with the experimental data. The reproducibility was assessed by the absolute relative logarithmic deviation (ARLD):

$$\left|\Delta \log_{10} x_2\right| = \left|\frac{\log_{10} x_2{}^{cal} - \log_{10} x_2{}^{\exp}}{\log_{10} x_2{}^{\exp}}\right| \tag{30}$$

Table 5.1 lists the ARLDs and their averages. The average ARLDs were 0.256, 0.272, 0.479, 0.190, and 0.146 % for methanol, MEG, DEG, TEG, and MDEA, respectively. Although this calculation method was originally developed to calculate Hg solubility in gaseous methane, ethane, and carbon dioxide at high pressures, it also could be applied to evaluate vapor-liquid-liquid equilibria between other liquid organic solvents and elemental Hg in the low-pressure range.

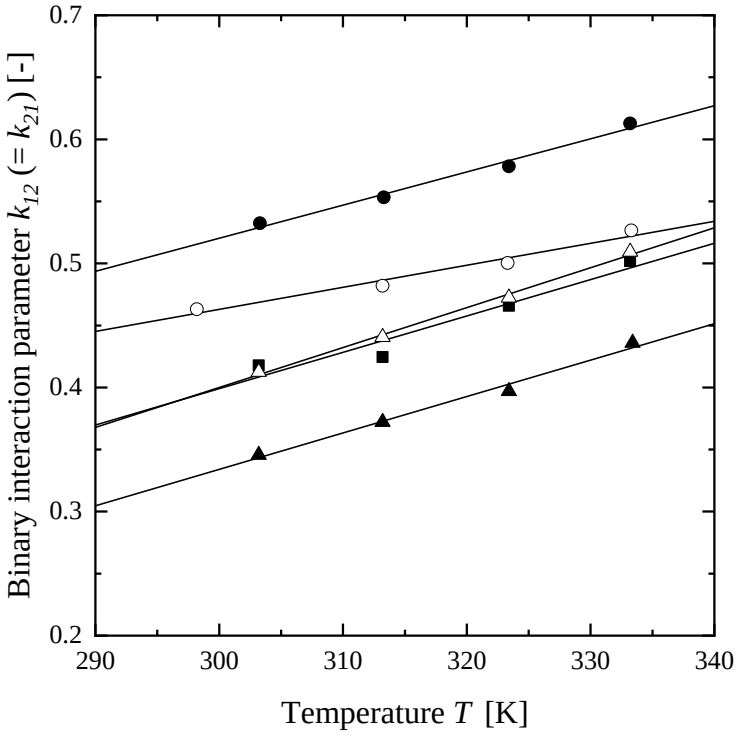

Fig. 5.10. Temperature dependence of binary interaction parameter in PR/PRSV-EOS; methanol-Hg, fitted (○); MEG-Hg, fitted (●); DEG-Hg, fitted (■); TEG-Hg, fitted (▲); MDEA-Hg, fitted, (△); Eq. (15) (——).

Table 5.4. Coefficients in binary interaction parameter for PR/PRSV-EOS

	Coefficients in binary interaction parameter k_{ij}		
	k_{ij}^0 (= k_{ji}^0) [-]	k_{ij}^1 (= k_{ji}^1) [K^{-1}]	k_{ij}^2 (= k_{ji}^2) [K]
methanol (1) – mercury (2)	-0.0696	0.00178	0.00
MEG (1) – mercury (2)	-0.2805	0.00267	0.00
DEG (1) – mercury (2)	-0.4801	0.00293	0.00
TEG (1) – mercury (2)	-0.5468	0.00294	0.00
MDEA (1) – mercury (2)	-0.5653	0.00322	0.00

Chapter 6 Conclusion

This chapter summarizes the findings of this study and provides main conclusion. Future prospects and further challenges are also discussed for future research.

The investigation of Hg solubility in gaseous natural gas components started with the experimental apparatus based on the flow method was constructed, then the saturated vapor pressure of Hg was measured for the validation of the apparatus. Next, the Hg solubility measurements for gaseous methane, ethane, carbon dioxide, and artificial natural gas, which simulated natural gas, were conducted. The investigation of Hg solubility in solvents for natural gas processing included the Hg solubility in methanol, MEG, DEG, TEG, and MDEA under atmospheric pressure. The main findings of this work are as follows:

- The mole fraction of Hg was decreased with the pressure up to 6 MPa in gaseous methane. Under the isobaric condition, the mole fraction of Hg increased with the temperature and followed the van't Hoff equation. The trends were similar to ethane, carbon dioxide, and artificial natural gas. The dissolution enthalpies evaluated from the van't Hoff plots were almost identical among methane, ethane, carbon dioxide, and artificial natural gas. Moreover, the enthalpies were the same as the enthalpy of vaporization of Hg calculated from the saturated vapor pressure of Hg. At the pressure close to the saturated dew point for ethane and carbon dioxide, the dissolution enthalpy was slightly decreased. These results suggested that the Hg and gas molecules will be isolated, and the interaction between gas molecules and Hg will not be substantial. The aggregation of Hg will be promoted in the vapor phase close to the dew point as well as in the supercritical fluid. These phenomena were similar to SLE if Hg had immiscibility with these compounds. Therefore, we consider that the mole fraction of Hg is increased at higher pressure.
- The mole fraction of Hg in MEG, DEG, TEG, and MDEA increased with the temperature and followed the van't Hoff equation. Among the four chemicals, the dissolution enthalpy was around 23 kJ· mol^{-1}. The value was far smaller than that in isobaric gases of methane, ethane,

and carbon dioxide, 61 $kJ \cdot mol^{-1}$. At the isothermal condition, the mole fraction was proportional to the number of their constituent atoms. In addition, the Hg solubilities in C5 to C8 and C10 of aliphatic hydrocarbons also followed this relationship. It can be utilized to predict the Hg solubility in heavy hydrocarbon impurities in natural gas and oil, especially for estimating the Hg solubility in pseudo-components of heavy hydrocarbons for process simulation of natural gas processing facilities [73].

- Conventional cubic EOS, such as the PR-EOS, could correlate the mole fraction of Hg in methane, ethane, and carbon dioxide with the assumption that the liquid Hg phase was a solid with fluidity. Then, the attractive parameter should be optimized for Hg by using the saturated vapor pressure of Hg. The correlations were acceptable and agreed well with the experimental data. The calculation method could also be applied to the artificial natural gas with the binary interaction parameters among the three binary constituents: methane–ethane, ethane–carbon dioxide, and carbon dioxide-methane. The PR-EOS could also be applied to Hg solubilities without modification in methanol, MEG, DEG, TEG, and MDEA by assuming vapor-liquid-liquid equilibrium (VLLE).

One of the most important findings in this research is that conventional cubic EOS could be applied to calculate the VLE and the VLLE, including liquid metal, such as elemental Hg. However, there are some technical challenges for future research. First is the expandability of the value of α in the PR-EOS. As discussed in **section 4.1.3**, the value of α in the PR-EOS was determined by considering the temperature dependence of α against the measured values of the saturated vapor pressure of Hg. As the reliability of α depends on the temperature range of the measurement of the saturated vapor pressure of Hg, the expandability of the value of α should be investigated. Second is the prediction of the reactivity of Hg in natural gas processing. As investigated in **section 5.1**, elemental Hg was easily oxidized by oxygen from the atmosphere, increasing its solubility. Oxygen possibly intrudes into natural gas processing facilities from supply lines of the gas processing chemicals, including glycols and amines. The reactivity of Hg should be investigated and modeled

to predict Hg distribution in natural gas processing facilities completely. Though further research is necessary, the prediction model for the Hg distribution can significantly contribute to managing Hg emission and preventing Hg pollution and occupational exposure of Hg to plant workers in natural gas processing facilities. Although this research focused on gas processing facilities, other applications will be expected. For example, the method will be capable to modeling phase behavior of molten metals, such as molten iron and impurities in converter furnace of steel manufacturing and float glass process using lead or tin, and to the development of liquid metal battery [74] which is expected to apply secondary battery for renewable energies.

Acknowledgements

I gratefully express my sincere gratitude to my academic supervisor, Professor Dr. Iwane Suzuki, for his continuous support of my research. His advice was invaluable for writing this thesis. I would like to express my gratitude to Professor Dr. Tomoya Tsuji from the Malaysia-Japan International Institute of Technology, Universiti Teknologi Malaysia for his considerable support from the start of this research project. He provided me with indispensable knowledge, advice, and motivation to conduct my research. I am also grateful to Assistant Professor Dr. Shinya Takahashi for sharing insightful suggestions to conduct my research and for his support of me in taking lectures in the doctoral program in Life Science Innovation. I would like to extend deep gratitude to Professor Dr. Sosaku Ichikawa for providing some valuable and very important comments to make my doctoral thesis meaningful. I would also like to thank Professor Dr. Hiroshi Inomata from the Research Center of Supercritical Fluid Technology, Tohoku University. He provided a lot of valuable comments to polish my research. Moreover, I must express my sincere gratitude to Emeritus Professor Dr. Katsumi Tochigi from the College of Science and Technology, Nihon University. He gave me a valuable opportunity to meet Professor Tsuji and start this research project.

My gratitude is also delivered to Dr. Takao Iwata, Mr. Hiroshi Akai, Mr. Takeshi Yoshida, and Mr. Atsushi Kobayashi from INPEX Corporation Technical Research Center for permitting and supporting my undertaking this research and for my entrance into the doctoral program in Life Science Innovation in the University of Tsukuba.

I express my special thanks to my colleagues, Mr. Takehiro Shibuya, Ms. Midori Kawasaki, and Ms. Machie Otsuka from INPEX Corporation Technical Research Center, for conducting many experiments at great efforts for this research. We could not have achieved this research outcome without their substantial contributions.

I would like to dedicate this thesis to my beloved family, my wife Keiko and my son Atsuki, and to thank for their continuous encouragement and support throughout my research and my life. I have made my doctoral research because of their emotional supports.

Finally, I would like to extend my gratitude to my father and my mother. They supported and watched over me in my good times and bad times. I was just about to be a university student when my mother passed away at the age of fifty. She was delighted to hear about my entrance to the university. After many long years, I think I have been able to return the favor to my father and mother by receiving my Ph. D. Also, continuing to work hard in the future becomes a tribute to the memory of my mother in heaven.

References

[1] Kinney, G.T., Skikda LNG Plant Solving Troubles, *Oil Gas J*., 73, 192-193 (1975).

[2] Bingham, M.D., Field Detection and Implications of Mercury in Natural Gas, *SPE Prod. Engineer.*, 5, 120-124 (1990).

[3] Leeper, J.E., Mercury—LNG's problem, *Hydrocarbon Processing*, 59, 237-240 (1980).

[4] Situmorang, M.S.M. and Muchlis, M., Mercury Problems in the Arun LNG Plant, 8th International Conference on LNG, Los Angeles, June 1986, session 2, paper 5 (1986).

[5] Santos, S., Mercury in Oxy-Coal Fired Power Plant with CO2 Capture. What is the real score?, 3rd IEAGHG International Oxy-Combustion Workshop, Yokohama, Japan, session 2a, March 5 (2008).

[6] Salva, C., Gallup, D., Mercury Removal Process Is Applied to Crude Oil of Southern Argentina, SPE-138333, SPE Latin American & Caribbean Petroleum Conference 2010, Lima, Peru (2010).

[7] UN Environment, Global Mercury Assessment 2018, UN Environment Programme, Chemicals and Health Branch Geneva, Switzerland (2019).

[8] AMPP/UN Environment, Technical Background Report for Global Mercury Assessment 2018, Arctic Monitoring and Assessment Programme, Oslo, Norway/UN Environment Programme, Chemicals and Health Branch Geneva, Switzerland (2019).

[9] Richardson, M.J., Rowlinson, J.S., The solubility of mercury in gases at high density, *Trans. Faraday Soc*., 55, 1333–1337 (1959).

[10] Jepson, W.B., Richardson, M.J., Rowlinson, J.S., The solubility of mercury in gases at moderate pressures, *Trans. Faraday Soc*., 53, 1586-1591 (1957).

[11] Butala, S.J.M., Wilson, G.M., Jasperson, L.V., Elemental Mercury Equilibrium in Selected Saturated Hydrocarbons, GPA Research Report RR-224, GPA Midstream Association, Tulsa, U.S. (2016).

[12] Chapoy, A., Ahmadi, P., Szczepanski, R., Zhang, X., Speranza, A., Yamada, J., Kobayashi, A., Elemental mercury partitioning in high pressure fluids part 1: Literature review and

measurements in single components, *Fluid Phase Equilib*., 520, 112660 (2020).

[13] Klehr, E.H., Voigt, A.F., Solubility of Metallic Mercury in Organic Solvents, Conference on the Use of Radioisotopes in the Physical Sciences and Industry, Copenhagen (1960).

[14] Kuntz, R.R., Mains, G.J., The Solubility of Mercury in Hydrocarbons, *J. Phys. Chem*., 68, 408-410 (1964).

[15] Choi, S.S., Tuck, D.G., A Neutron-activation Study of the Solubility of Mercury in Water, *J. Chem. Soc*., 4080–4088 (1962).

[16] Spencer, J.N., Voigt, A.F., Thermodynamics of the solution of mercury metal. I. Tracer determination of the solubility in various liquids, *J. Phys. Chem.*, 72, 464-470 (1968).

[17] Glew, D.N., Hames, D A., Aqueous Nonelectrolyte Solutions. Part X. Mercury Solubility in Water, *Can. J. Chem*., 49, 3114–3118 (1971).

[18] Vogel, A. Gjaldebaek, J.C., No title, *Arch. Pharm. Chem. Sci. Ed*., 2, 25-29 (1974).

[19] Onat, E., Solubility studies of metallic mercury in pure water at various temperatures, *J. Inorg. Nucl. Chem*., 36, 2029–2032 (1974).

[20] Sorokin, V.I., Solubility of mercury in water over the temperature-pressure range 300–500°C and 500–1000 atm. *Doklady Akademii Nauk SSSR*, 213 (4), 852–5, (1978).

[21] Okouchi, S., Sasaki, S., The Measurement of the Solubility of Metallic Mercury in Hydrocarbons by Means of the Cold-vapor Atomic Absorption Method. *Bull. Chem. Soc. Jpn.*, 54, 2513-2514 (1981).

[22] Okouchi, S., Sasaki, S., Chemical and Physical Behavior of Mercury in Water I, Report of the College of Engineering of Hosei University, 22, 57-106 (1983).

[23] Migdisov, A.A., Kister, P., Williams-Jones, A.E., An Experimental Study of the Solubility of Liquid Mercury in Octane and Dodecane at Temperatures up to 200°C, *J. Conf. Abstr*., 5, 706 (2000).

[24] Miedaner, M.M., Migdisove, A.A., Williams-Jones, A.E., Solubility of metallic mercury in octane, dodecane and toluene at temperatures between 100°C and 200°C. *Geochim. Cosmochim.*

Ac., 69, 5511-5516 (2005).

[25] Bloom, N.S., Gallup, D., On the Solubility of Mercury in Liquid Hydrocarbons, 2010 AIChE Spring Meeting and 6th Global Congress on Process Safety, San Antonio, U.S. (2010).

[26] Gallup, D.L., O'Rear, D.J., Radford, R., The behavior of mercury in water, alcohols, monoethylene glycol and triethylene glycol. *Fuel*, 196, 178-184 (2017).

[27] Marsh, K.N., Bevan, J.W., Holste, J.C., McFarlane, D.L., Eliades, M., Rogers, W.J., Solubility of Mercury in Liquid Hydrocarbons and Hydrocarbon Mixtures, *J. Chem. Eng. Data*, 61, 2805-2817 (2016).

[28] Corns, W.T., de Feo, G., Dexter, M.A., Solubility of Mercury in Selected Gas Processing Solvents, GPA Midstream Research Report RR-246, GPA Midstream Association, Tulsa, U.S. (2020).

[29] Sanemasa, I., The Solubility of Elemental Mercury Vapor in Water, *Bull. Chem. Soc. Jpn.*, 48, 1795-1798 (1975).

[30] Li, J., Zhao, Y., Yan, Q., Duan, Y., Wang, S., Zhang, X., Han, Z., Measurement of Elemental Mercury Solubility in Natural Gas Dehydrating Solvents, *IOP Conf. Series: Mater. Sci. Eng.*, 394, 022060 (2018).

[31] Huber, M.L., Laesecke, A., Friend, D.G., The Vapor Pressure of Mercury, NISTIR6643, National Institute of Standard and Technology (NIST), Boulder, U.S. (2006).

[32] Huber, M.L., Laesecke, A., Friend, D.G., Correlation for the vapor pressure of mercury, *Ind. Eng. Chem. Res*., 45, 7351-7361 (2006).

[33] Dumarey, D., Brown, R.J.C., Corns, W.T., Brown, A.S., Stockwell, P.B., Elemental mercury vapour in air: the origins and validation of the 'Dumarey equation' describing the mass concentration at saturation, *Accred. Qual. Assur*., 15, 409-414 (2010).

[34] International Standardization Organization, ISO 6978-2:2003, Natural gas—determination of mercury—Part 2: sampling of mercury by amalgamation on gold/platinum alloy, ISO, Geneva, Switzerland (2003).

[35] Brown, R.J.C., Brown, A.S., Yardley, R.E., Corns, W.T., Stockwell, P.B., A practical uncertainty budget for ambient mercury vapour measurement, *Atmos. Environ.*, 42, 2504-2517 (2008).

[36] Edmonds, B., Moorwood, R.A.S., Szczepanski, R., Mercury Partitioning in Natural Gases and Condensates, GPA European Chapter Meeting, London (1996).

[37] Smit, C.J., Meijer, J., Hendriks, E.M., Mercury, the Volatile Surprise in Gas Processing, 83rd GPA Annual Convention, New Orleans, U.S. (2004).

[38] Mentzelos, C., Modelling of Mercury (Hg) Distribution in Natural Gas Mixtures, MSc Thesis of National Technical University Athens (2015).

[39] Koulocheris, V., Louli, V., Panteli, E., Skouras, S., Voutsas, E., Modelling of elemental mercury solubility in natural gas components, *Fuel*, 233, 558-564 (2018).

[40] Reichardt, H., Bonhoeffer, K.F., The absorption spectrum of dissolved mercury, *Z. Phys*., 67, 780–789 (1931).

[41] Clever, H.L., (Ed.), Mercury in Liquids, Compressed Gases, Molten Salts and Other Elements, IUPAC Solubility Data Series, Pergamon Press, Oxford, U.K. (1987).

[42] Spencer, J.N., Voigt, A.F., Thermodynamics of the solution of mercury metal. III. Dimethylcyclohexanes and Alcohols as Solvents, *J. Phys. Chem.*, 72, 1913-1917 (1968).

[43] Khalifa, M., Lue, L., A group contribution method for predicting the solubility of mercury, *Fluid Phase Equilib.*, 432, 76-84 (2017).

[44] Polishuk, I., Nakonechny, F., Brauner, N., Predicting phase behavior of metallic mercury in liquid and compressed gaseous hydrocarbons, *Fuel*, 174, 197-205 (2017).

[45] Riddick, J.A., Bunger, W.B., Sakano, T.K., Organic Solvents Physical Properties and Methods of Purification, 4th edition, Wiley, New York (1986).

[46] Al-Ghawas, H.A., Hagewlesche, D.P., Ruiz-Ibanez, G., Sandall, O.C., Physicochemical Properties Important for Carbon Dioxide Absorption in Aqueous Methyldiethanolamine, *J. Chem. Eng. Data*, 34, 385-391 (1989).

[47] Peng, D.Y., Robinson, D.B., A New Two-Constant Equation of State, *Ind. Eng. Chem. Fund.*,

15, 59-64 (1976)

[48] Yaws, C.L., Chemical Properties Handbook, McGraw-Hill, New York (1999).

[49] Poling, B.E., Prausniz, R.J.M., O'Connell, J.P., The properties of Gases & Liquids, 5th edition, McGraw -Hill, New York (2001).

[50] Stryjek, R., Vera, J.H., PRSV: An Improved Peng-Robinson Equation of State for Pure Compounds and Mixtures, Can. *J. Chem. Eng*., 64, 323-333 (1986).

[51] Nikitin, E.D., Popov, A.P., Critical temperatures and pressures of ethylene glycols. *Fluid Phase Equilib*. 472, 56-61 (2018).

[52] NIST Chemistry WebBook, SRD 69, Thermophysical Properties of Fluid Systems, National Institute of Standard and Technology (NIST), Boulder U.S, https://webbook.nist.gov/chemistry/fluid/.

[53] Ernsberger, F.M., Pitman, H.W., New absolute manometer for vapor pressures in the micron range, *Rev. Sci. Instrum*., 26, 584-589 (1955).

[54] Hildenbrand, D.L., Hall, W.F., Ju, F., Potter, N.D., Vapor pressures and vapor thermodynamic properties of some lithium and magnesium halides, *J. Chem. Phys*., 40, 2882-2890 (1964).

[55] Hill, C.F., Measurement of mercury vapor pressure by means of the Knudsen pressure gauge, *Phys, Rev*., 20, 259-266 (1922).

[56] McHugh, M., Paulaltis, M.E., Solid-Solubility of Naphthalene and Biphenyl in Supercritical Carbon Dioxide, *J. Chem. Eng. Data*, 25, 326-329 (1980).

[57] Hasegawa, S., Naoe, T., Futakawa, M., Solubility of helium in mercury for bubbling technology of the spallation neutron mercury target, *J. Nucl. Mater*., 398, 189-192 (2010).

[58] Sandler, S.I., Chemical and Engineering Thermodynamics, John Willy & Sons, New York, 1989.

[59] N. Orbey, S. I. Sandler, Vapor-liquid Equilibrium of Polymer Solutions Using a Cubic Equation of State, *AIChE J*., 40, 1203-1209 (1994).

[60] Guputa, M.K., Gardner, G.C., Hegarty, M.J., Kidnay, A.J., Liquid-vapor equilibriums for the N_2 + CH_4 + C_2H_6 system from 260 to 280 K, *J. Chem. Eng. Data*, 25, 313-318 (1980).

[61] Raabe, G., Janisch, J., Koehler, J., Experimental studies of phase equilibria in mixtures relevant for the description of natural gases, *Fluid Phase Equilib*., 185, 199-208 (2001).

[62] Janisch, J., Raabe, G., Köhler, J., Vapor−Liquid Equilibria and Saturated Liquid Densities in Binary Mixtures of Nitrogen, Methane, and Ethane and Their Correlation Using the VTPR and PSRK GCEOS, *J. Chem. Eng. Data*, 52, 1897-1903 (2007).

[63] Wei, M. S.-W., Brown, T.S., Kidnay, A.J., Slone, E.D., Vapor + Liquid Equilibria for the Ternary System Methane + Ethane + Carbon Dioxide at 230 K and Its Constituent Binaries at Temperatures from 207 to 270 K, *J. Chem. Eng. Data*, 40, 726-731 (1995).

[64] Brown, T.S., Slone, E.D., Kidnay, A.J., Vapor-liquid equilibria in the nitrogen + carbon dioxide + ethane system, *Fluid Phase Equilib*., 51, 299-313 (1989).

[65] Ohgaki, K., Katayama, T., Isothermal vapor-liquid equilibrium data for the ethane—carbon dioxide system at high pressures, *Fluid Phase Equilib*., 1, 27-32 (1977).

[66] Davalos, J., Anderson, W.R., Phelps, R.E., Kidnay, A.J., Liquid-Vapor Equilibria at 250.00 K for Systems Containing Methane, Ethane, and Carbon Dioxide, *J. Chem. Eng. Data*, 21, 81-84 (1976).

[67] Somait, F.A., Kidnay, A.J., Liquid-vapor equilibriums at 270.00 K for systems containing nitrogen, methane, and carbon dioxide, *J. Chem. Eng. Data*, 23, 301-305 (1978).

[68] Al-Sahhaf, T.A., Kidnay, A.J., Sloan, E.D., Liquid + vapor equilibriums in the nitrogen + carbon dioxide + methane system, *Ind. Eng. Chem. Fundam*., 22, 372-380 (1983).

[69] Donnely, H.G., Katz, D.L., Phase Equilibria in the Carbon Dioxide–Methane System, *Ind. Eng. Chem. Fundam*., 46, 511-517 (1954).

[70] Arai, Y., Kaminishi, G., Saito, S., The Experimental Determination of the P-V-T-X Relation for the Carbon Dioxide-Nitrogen and the Carbon Dioxide-Methane Systems, *J. Chem. Eng. Japan*, 4, 113-121 (1971).

[71] Xu, N., Dong, J., Wang, Y., Shi, J., High pressure vapor liquid equilibria at 293 K for systems containing nitrogen, methane and carbon dioxide, *Fluid Phase Equilib*., 31, 175-186 (1992).

[72] Clever, H.L., Iwamoto, M., Solubility of Mercury in Normal Alkanes, *Ind. Eng. Chem. Res*., 26, 336-337 (1987).

[73] Katz, D.L., Brown, G.G., Vapor Pressure and Vaporization of Petroleum Fractions, *Ind. Eng. Chem*., 25, 1373-1384 (1933).

[74] Ding, Y., Guo, X., Yu, G., Next-Generation Liquid Metal Batteries Based on the Chemistry of Fusible Alloys, *ACS Cent. Sci*., 6, 1355-1366 (2020).

APPENDIX I: Publication List and Presentation in Conference and Workshop

(Publication, related to this thesis)

[1] **Yamada, J.**, Kawasaki, M., Otsuka, M., Kobayashi, A., Tsuji, T., Measurement and Modeling of Mercury Solubility in Methanol, Glycols, and *N*-methyldiethanolamine, *J. Solution Chem.*, 50, 968–982 (2021).

[2] **Yamada, J.**, Shibuya, T., Kobayashi, A., Tsuji, T., Mercury solubility measurements in natural gas components at high pressure, *Fluid Phase Equilib.,* 506, 112342 (2020).

(Publication, related to international project)

[3] Chapoy, A., Ahmadi, P., **Yamada, J.**, Kobayashi, A., Szczepanski, R., Zhang, X., Speranza, A., lemental mercury partitioning in high pressure fluids part 2: Model validations and measurements in multicomponent systems, *Fluid Phase Equilib.*, 523,112775 (2020).

[4] Chapoy, A., Ahmadi, P., Szczepanski, R., Zhang, X., Speranza, A., **Yamada, J**., Kobayashi, A., Elemental mercury partitioning in high pressure fluids part 1: literature review and measurements in single components, *Fluid Phase Equilib.,* 520, 112660 (2020).

(Publication, others)

[5] 山田淳也，天然ガス開発にまつわる水銀の話―資源開発会社での研究開発活動を交えて―，天然ガス, 2, 10-18 (2021).

[6] 山田淳也，石油業界における水銀を取り巻く環境とその対応（第 2 回）原油・天然ガスにおける水銀への対応-資源開発会社での研究開発活動，ペトロテック, 43, 714-718(2020).

(Presentation at Conferences)

[7] 山田淳也, 渋谷健広, 川崎緑, 大塚町恵, 小林淳, 辻智也, 天然ガス処理プロセスにお

ける水銀の分配予測技術, 石油学会函館大会（第 51 回石油・石油化学討論会）, 函館 (hybrid) (2021).

[8] **Yamada, J.,** Kawasaki, M., Otsuka, M., Kobayashi, A., Tsuji, T., Measurement and Modelling of Mercury Solubility in Glycols and Amine, International Symposium on Solubility Phenomena and Related Equilibrium Process (ISSP) 19, Albuquerque (on-line), U. S. (2021).

[9] Tsuji, T, **Yamada, J**., Kawasaki, M., Otsuka, M., Kobayashi, A., Mercury solubility measurements in glycols and amines for natural gas processing plant 2021 9th International Symposium on Molecular Thermodynamics and Molecular Simulation (MTMS '21), Sendai (on-line), Japan (2021).

[10] Tsuji, T., Shibuya, T., **Yamada, J**., Kobayashi, A., Saturated vapor pressure of elemental mercury and mercury solubility in natural gas components at high pressures, International Chemical Engineering Symposia 2021, Tokyo (on-line) (2021).

[11] **山田淳也,** 渋谷健広, 辻智也, 小林淳, 高圧メタンガスへの微量水銀溶解度測定と状態方程式による推算, 第 40 回日本熱物性学会シンポジウム, 長崎 (2019).

[12] **Yamada, J.,** Technical Challenges against Mercury Issues on Oil and Gas Production, SPE/JAPT WORKSHOP: Innovations in Natural Gas – Development, Storage, Transportation and Utilisation, Tokyo (2019).

[13] **Yamada, J.**, Shibuya, T., Kobayashi, A., Tsuji, T., An Apparatus for Mercury Solubility Measurement in Gaseous Natural Gas Components at High Pressures, Properties and Phase Equilibria for Product and Process Design (PPEPPD) 2019, Vancouver, Canada (2019).

(Lecture at Workshop)

[14] **山田淳也**, 原油・天然ガス生産における水銀への対応 ―天然ガス成分への気相中水銀溶解度の測定とモデリング検討―, 第 2 7 回「化学工学物性定数の最近の動向」講演会―社員教育のための物性の基礎と実践―, 東京 (2019).

APPENDIX II: Modeling of Hg Distribution in Natural Gas Processing Facility

Since some parts of the result of the actual Hg distribution in natural gas processing facilities are containing confidential data only used in INPEX Corporation, they were not described in the main body of the thesis. The data was disclosed here as possible as INPEX Corporation was approved.

II-1. Experimental Section

II-1.1 Sampling site

The sampling site for the investigation of Hg distribution was a three-phase separator in a natural gas processing facility. The pressure and the temperature of the separator were 7.645 MPa and 309.63 K, respectively.

II-1.2 Sampling and analytical method of gas samples

Natural gas samples were collected by 5 L or 10 L of Tedlar® gas sampling bags (GL Sciences Inc., Tokyo) from sampling ports of gas lines. Prior to the sampling, natural gas was purged for 5 minutes at 1 L· Nm^{-3} of flow rate. Then, natural gas was collected in the sampling bag at 1 L· Nm^{-3} of flow rate. The sampling valve was continuously heated during the sampling by a heating element made of quicklime to avoid Hg drop out by Joule-Thomson effect. After the samplings, Hg in the natural gas samples were immediately collected by passing through Hg collector tubes (Nippon Instruments, Tokyo) based on gold amalgamation method, while volume of natural gas passed through the tubes was measured by a wet gas meter (Shinagawa Co., Tokyo, W-NK-0.5) with a minimum indicator volume of 1 cm^3. Then Hg amounts in the Hg collector tubes were measured by a total Hg analyzer for gas sample (Nippon Instruments, Tokyo, WA-4) based on the CVAAS.

II-1.3 Sampling and analytical method of pressurized liquid samples

Pressurized liquid samples were collected 500 mL of 1 L of stainless sample cylinders made of stainless steel 316 (Swagelok Co., Solon, U.S.) with SilcoNert2000 inert coating (SilcoTek Co., Bellefonte, U.S.) from sampling ports of gas lines. Liquid samples were well purged before the samplings. After the samplings, the valve in the cylinder was carefully opened, then a gas flew from the cylinder was collected Tedlar® gas sampling bag. After the gas collection, a depressurized liquid in the cylinder was collected a PTFE sample bottle. Hg content in both the depressurized gas and the liquid was measured the total Hg analyzer for gas (Nippon Instruments, Tokyo, WA-4) and the total Hg analyzer for liquid (Nippon Instruments, Tokyo, MA-3000), respectively.

II-1.4 Modeling

The Hg partitioning calculation in the separator was performed by Aspen HYSYS V10 (Aspen Technology Inc., Bedford, U.S.). Cubic Plus Association (CPA) EOS was used as the prediction model. Binary interaction parameters (BIPs) in the cubic term of CPA-EOS between mercury and some components (nitrogen, carbon dioxide, ethane, propane, iso-butane, n-pentane, and water) were tuned to fit the experimental data or literature data of Hg solubility in each component by the data regression system of Aspen Plus V10 (Aspen Technology Inc., Bedford, U.S.). Other BIPs in the cubic term and in the association term of CPA-EOS were used as the default values of HYSYS. Critical pressure, critical temperature, and acentric factor of the pseudo components (C6*, C7*, C8*, C9*, C10-12*, C13-16*, C17-20*, C21-27*, and C28+*) were tuned to fit the phase envelop of the separator inlet fluid by Multiflash 7.0 (KBC Advanced Technologies Ltd., London). The BIPs in the cubic term of CPA-EOS between mercury and the pseudo components were estimated based on the mercury solubility of C6 to C8, and C10 aliphatic hydrocarbons.

II-2. Results

Figure A-II-1 shows the results of the Hg distribution in the three-phase separator both the

actual measurements and the calculation by HYSYS. The condensate and the water calculations showed good agreement with the experimental measurements.

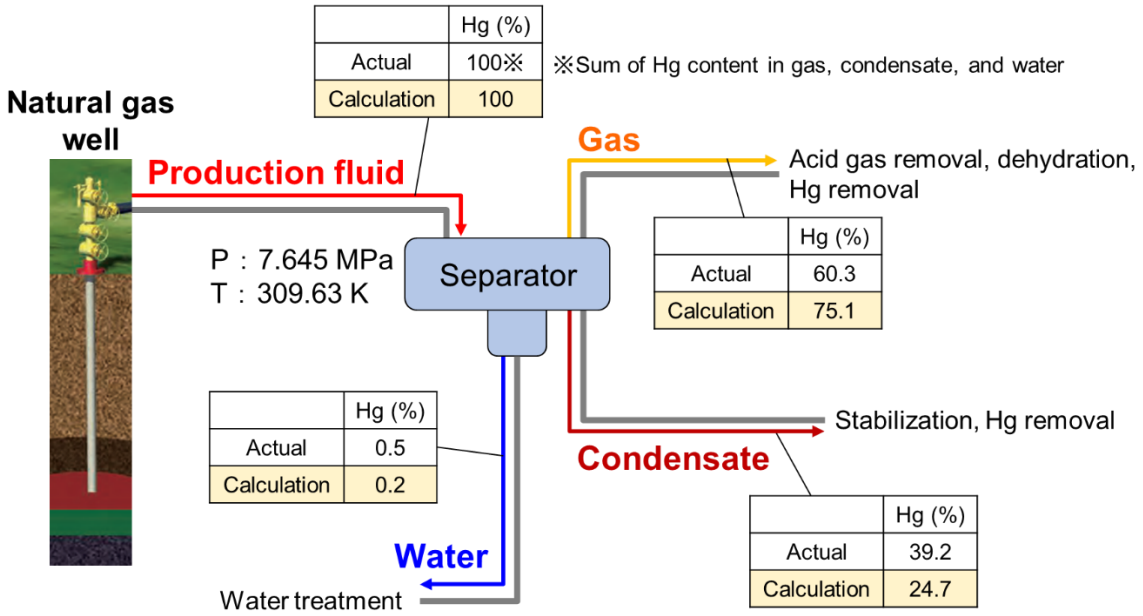

Fig. A-II-1. Results of Hg distribution in the three-phase separator.